PHYSICAL REVIEW D **85,** 023531 (2012)

Non-Gaussianity from step features in the inflationary potential

Peter Adshead,[1] Cora Dvorkin,[1,2,3] Wayne Hu,[1,4] and Eugene A. Lim[5]

[1]*Kavli Institute for Cosmological Physics, Enrico Fermi Institute, University of Chicago, Chicago, Illinois 60637, USA*
[2]*Department of Physics, University of Chicago, Chicago, Illinois 60637, USA*
[3]*School of Natural Sciences, Institute for Advanced Study, Princeton, New Jersey 08540, USA*
[4]*Department of Astronomy and Astrophysics, University of Chicago, Chicago, Illinois 60637, USA*
[5]*Department of Applied Maths and Theoretical Physics, University of Cambridge, Cambridge CB3 0HA, United Kingdom*

(Received 21 October 2011; published 26 January 2012)

We provide analytic solutions for the power spectrum and bispectrum of curvature fluctuations produced by a step feature in the inflaton potential, valid in the limit that the step is short and sharp. In this limit, the bispectrum is strongly scale dependent and its effective nonlinearity attains a large oscillatory amplitude. The perturbations to the curvature power spectrum, on the other hand, remain a small component on top of the usual spectrum of fluctuations generated by slow roll. We utilize our analytic solutions to assess the observability of the predicted non-Gaussian signatures and show that, if present, only very sharp steps on scales larger than ~ 2 Gpc are likely to be able to be detected by Planck. Such features are not only consistent with WMAP7 data, but can also improve its likelihood by $2\Delta \ln L \approx 12$ for two extra parameters, the step location and height. If this improvement were due to a slow roll violating step as considered here, a bispectrum or corresponding polarization power spectrum detection would provide definitive checks as to its primordial origin.

DOI: 10.1103/PhysRevD.85.023531 PACS numbers: 98.80.Cq, 98.70.Vc

I. INTRODUCTION

In this paper we employ the generalized slow roll (GSR) approach [1–4] to consider the bispectrum of primordial fluctuations generated by a transient violation of slow roll due to a step feature in the inflaton potential. While earlier works in the field have considered the non-Gaussianity from these models, here we explore a hitherto unexplored region of the parameter space where the step in the potential becomes sharp. This region of parameter space is near the so-called ''decoupling'' limit where the perturbations in the power spectrum due to the step remain small while higher order N-point functions are parametrically enhanced [5,6].

Features in the inflationary potential have a long history [7]. They came into vogue as a possible explanation for the apparent low multipole glitch at $\ell \sim 20$–40 in the angular spectrum of the cosmic microwave background (CMB) radiation [8–11]. If such a feature arises as a result of a glitch in the primordial potential then corresponding features should arise in the electric-type polarization pattern of the CMB [11]. More generally, failure to detect consistent patterns in the polarization may even be considered evidence against a single adiabatic degree of freedom as the source of the primordial perturbations [4].

Beyond two-point statistics such as the angular temperature and polarization power spectra, it is well known that such a glitch in the potential leads to higher N-point functions which are enhanced relative to those generated by the otherwise smooth background [12–16]. However, as was shown in our earlier work [17], the bispectrum, or three-point function produced by a step feature that best fits the glitch in the WMAP data, [4,11] falls short of detectability by a very wide margin.

In this work we investigate the space of parameters that corresponds to the step becoming short and sharp. As we will see, in this limit, the perturbations in the power spectrum remain small while the reduced bispectrum or effective nonlinearity $f_{\rm NL}(k)$ becomes large. Despite this seeming largeness, the bispectrum remains difficult to detect due to its oscillatory form. Nonetheless, for a sufficiently sharp step at sufficiently large scales, an observably large non-Gaussianity is compatible with current power spectrum constraints.

This paper is organized as follows: In Sec. II we derive approximate solutions to the evolution of the inflaton on an inflationary potential that undergoes a sharp downward step. These solutions yield analytic expressions for the perturbation to the curvature power spectrum in Sec. III. In Sec. IV we review the formalism used to calculate the bispectrum from which we obtain approximate analytic solutions. The constraints that the WMAP 7 year power spectrum data place on the sharp-step region of parameter space in Sec. V inform the prospects for the detection of the bispectrum in a cosmic variance limited CMB experiment in Sec. VI. We summarize our findings in Sec. VII.

Some related but separate studies are presented in the Appendixes. In Appendix A, we investigate the real space analogs of the power spectrum and bispectrum of curvature fluctuations generated by a sharp-step feature. In Appendix B, we calculate the leading order slow roll corrections to our analytic solutions. Finally in Appendix C, we demonstrate that our analytic solutions are approximately separable.

Throughout the paper we work in units where the reduced Planck mass $M_{\rm Pl} = (8\pi G)^{-1/2} = 1$ as well as $\hbar = c = 1$.

II. BACKGROUND SOLUTION

We consider a homogeneous scalar field minimally coupled to gravity with a potential of the form

$$V(\phi) = V_0(\phi)\left[1 + cF\left(\frac{\phi_f - \phi}{d}\right)\right], \tag{1}$$

where the potential V_0 supports slow roll inflation in the limit where $c \to 0$, and $F(x)$ is a function which transitions from -1 to $+1$ as its argument passes through $x = 0$ from above with a characteristic width $\Delta x = 1$. Thus the potential characterizes a step of height $2c$ and half-width d. When an explicit choice is required, we will take

$$F(x) = -\tanh(x) \tag{2}$$

as an example in the following sections.

The scalar field obeys the usual equation of motion on the background

$$\ddot{\phi} + 3H\dot{\phi} + \frac{dV}{d\phi} = 0, \tag{3}$$

where $H = \dot{a}/a$ is the Hubble parameter, and an overdot represents a derivative with respect to cosmic time.

In the limit in which the step is short, $c \ll 1$, its presence in the potential will have only a small effect on the evolution of the inflaton. Specifically, as long as the change in the potential as the field rolls across the step is small compared with the kinetic energy of the background field, then we can think of the effect of the step as a perturbation on the evolution of ϕ on the potential V_0. As the field crosses the step a potential energy $\Delta V \approx cV$ is converted into kinetic energy. Comparing this with the kinetic energy of the inflaton rolling on the background we find

$$\frac{2\Delta V}{\dot{\phi}^2} \approx \frac{4cV}{\dot{\phi}^2} \approx 6\frac{c}{\epsilon_H}, \tag{4}$$

where we have introduced the slow roll parameter

$$\epsilon_H \equiv -\frac{\dot{H}}{H^2} = \frac{\dot{\phi}^2}{2H^2}. \tag{5}$$

Whenever

$$c \ll \epsilon_H/6, \tag{6}$$

we can treat the effect of the step as a small perturbation on the background described by V_0.

With this limit in mind, we look to solve Eq. (3) iteratively as follows: taking $6c \ll \epsilon_H$, we split the field into a piece zeroth order in c and pieces which we take to be higher order in c

$$\phi = \phi_0 + \phi_1 + \cdots, \qquad \epsilon_H = \epsilon_0 + \epsilon_1 + \cdots. \tag{7}$$

In this expression, ϕ_0 characterizes the behavior of the field in the absence of the step, i.e. on the potential V_0, while ϕ_1 is the perturbation which is taken to be linear in c, and $\cdots$ denotes terms higher order in an expansion in

$$\mathcal{C} \equiv \frac{6c}{\epsilon_0}. \tag{8}$$

While the condition in Eq. (6) requires that $\dot{\phi}_1$ remains small, it places no restriction on higher derivatives. In particular, we will see that by making the step sharp we can make the acceleration and jerk of the field ϕ_1 arbitrarily large.

It proves useful to write the equation of motion for the perturbation, ϕ_1, using the value of the background field ϕ_0 as the independent variable. The condition $6c \ll \epsilon_0$ requires that $\dot{\phi}_0 \neq 0$ and $\phi_0(t)$ evolve monotonically in the vicinity of the step which ensures that ϕ_0 is a suitable time variable. Given that on the background potential V_0, the slow roll approximation yields $\epsilon_0 \approx (V'/V)^2/2$ and assuming that $\epsilon_0 \approx$ const (and so not $\ll |V''/V|$), we obtain the equation of motion for ϕ_1 as

$$\frac{d}{d\phi_0}\left(e^{-(3\phi_0/\sqrt{2\epsilon_0})}\frac{d\phi_1}{d\phi_0}\right) = -\frac{\mathcal{C}}{4}\left(\frac{\sqrt{2\epsilon_0}}{2}F + \frac{dF}{d\phi_0}\right)e^{-(3\phi_0/\sqrt{2\epsilon_0})}, \tag{9}$$

where the subscript 0 denotes quantities to be evaluated on the unperturbed ($c = 0$) background and we have dropped some terms that are suppressed by slow roll parameters evaluated on the unperturbed background.

For small sharp steps, the $dF/d\phi_0$ term in Eq. (9) dominates and

$$e^{-(3\phi_0/\sqrt{2\epsilon_0})}\frac{d\phi_1}{d\phi_0} \approx -\frac{\mathcal{C}}{4}\int d\phi_0 \frac{dF}{d\phi_0}e^{-(3\phi_0/\sqrt{2\epsilon_0})} + \text{const.} \tag{10}$$

The exponential in the integrand is slowly varying across the width of the step and may be evaluated at ϕ_f and taken out of the integral. Furthermore the integration constant is set by the boundary condition that $d\phi_1/d\phi_0 = 0$ before crossing the step and so

$$\frac{d\phi_1}{d\phi_0} \approx \frac{\mathcal{C}}{4}e^{-(3/\sqrt{2\epsilon_0})(\phi_f - \phi_0)}\left[1 - F\left(\frac{\phi_f - \phi_0}{d}\right)\right]. \tag{11}$$

In principle, we could further integrate to find ϕ_1; however, this is not necessary for this work.

The final step is to reference this solution to conformal time rather than the background field. Since the perturbation ϕ_1 is only important for a short period of time, the variation of the unperturbed ($c = 0$) slow roll parameters is negligible. In this approximation, the evolution of the background in conformal time is very simple

$$\frac{d\phi_0}{d\ln\eta} = \pm\sqrt{2\epsilon_0} \approx \text{const},$$
$$\phi_0 - \phi_f = \pm\sqrt{2\epsilon_0}\ln(\eta/\eta_f), \tag{12}$$

where the sign should be chosen depending on the direction the field is rolling—i.e. whether one is in a large or small field inflationary model and one is rolling toward or away from the origin. In this work, we have large field inflationary models in mind, e.g. $V_0 = \frac{1}{2}m^2\phi^2$ and will take the positive sign.

With these relations, we can explicitly solve for the first order changes to the slow roll parameters as a function of conformal time. The slow roll parameters are defined by Eq. (5) and

$$\eta_H = -\frac{\ddot{\phi}}{\dot{\phi}H}, \qquad \delta_2 = \frac{\dddot{\phi}}{\dot{\phi}H^2}. \tag{13}$$

Using the results above, we divide the slow roll parameters into a background part and a part that is linear in the perturbation, $\eta_H = \eta_0 + \eta_1$ and $\delta_2 = \delta_{2,0} + \delta_{2,1}$,

$$\epsilon_1 = \frac{\mathcal{C}}{2}\epsilon_0\left(\frac{\eta}{\eta_f}\right)^3\left\{1 - F\left[-\frac{\sqrt{2\epsilon_0}}{d}\ln\left(\frac{\eta}{\eta_f}\right)\right]\right\},$$
$$\eta_1 = \frac{\epsilon_1'}{2\epsilon_0}, \qquad \delta_{2,1} = \eta_1'. \tag{14}$$

Here and below primes denote derivatives with respect to $\ln\eta$. Notice that ϵ_1 remains a tiny correction to the already small ϵ_0, of order $\mathcal{O}(\mathcal{C})$, as expected. On the other hand, in principle η_1 and $\delta_{2,1}$ can be arbitrarily large due to the presence of the $1/d$ factors from the derivatives. In what follows we will see that these give rise to a large and strongly scale dependent bispectrum.

In deriving these results, we have assumed that the perturbation series converges. At first, it may seem that this requirement would impose a restriction on the width of the step, d, due to successively expanding the $dV/d\phi$ term in Eq. (3) at each order in perturbation theory. However, note that by iteration, these terms are always multiplied by the previous order in the perturbation series

$$\frac{d}{d\phi_0}\left(e^{-(3\phi_0/\sqrt{2\epsilon_0})}\frac{d\phi_n}{d\phi_0}\right) = -\frac{\mathcal{C}}{4}\frac{d^nF}{d\phi_0^n}\phi_{n-1}e^{-(3\phi_0/\sqrt{2\epsilon_0})}. \tag{15}$$

Around the step, the derivatives of F carry factors of d^{-n} for a $\Delta\phi_0$ interval of order d. Thus in this neighborhood, the integrals over ϕ_0 give contributions of order d, ϕ_1 is of order $(\mathcal{C}d)$, and ϕ_n is of order $(\mathcal{C}d)^n$. With these relations $d\phi_n/d\phi_0$ is order $\mathcal{C}^n$ there and is independent of d as $d \to 0$. The corrections to the slow roll parameter are then also strongly convergent as long as $\mathcal{C} \ll 1$.

Another way of seeing why the series is convergent as we take $d \to 0$ is to realize that these perturbative corrections amount to small shifts in when the inflaton crosses the sharp feature and hence unobservable changes in the temporal location of features in the slow roll parameters.

In fact for the purpose of computing the shapes of these features, we can always define the position of the step in some arbitrary choice of the zero point in $\ln\eta$ or e-folds to be the same as that of the background to all orders. The background has an approximate time translation symmetry (broken only weakly by $\dot{H} \neq 0$) and so there is no dynamical consequence to this choice. As $d \to 0$ the step becomes sharp and changes to the potential are no longer well approximated by a Taylor series for finite perturbations in field value. But making use of the approximate time translation invariance of the background, we have defined these away. It then follows that the linear expansion in $\mathcal{C}$ remains valid in the limit $d \to 0$. We shall see in the next sections that nonlinear scalings of this type can be used to extend the analytic solutions to the power spectrum and bispectrum out to $\mathcal{C} \sim 1$.

III. CURVATURE POWER SPECTRUM

In Sec. III A, we use the background solution of the last section to derive an analytic form for the curvature power spectrum of the step potential. We test this analytic form against numerical calculations in Sec. III B and show that it can be extended to order unity features with a nonlinear rescaling of parameters.

A. Analytic power spectrum solution

In the generalized slow roll approximation, the power spectrum of curvature fluctuations $\Delta^2_{\mathcal{R}} = k^3P_{\mathcal{R}}/2\pi^2$ is given to leading order in the source function by [2]

$$\ln\Delta^2_{\mathcal{R}}(k) = G(\ln\eta_*) + \int_{\eta_*}^{\infty}\frac{d\eta}{\eta}W(k\eta)G'(\ln\eta), \tag{16}$$

where the source function

$$G(\ln\eta) = -2\ln f + \tfrac{2}{3}(\ln f)', \tag{17}$$

with

$$f = \frac{\sqrt{8\pi^2\epsilon_H}}{H}(aH\eta). \tag{18}$$

Recall that primes denote derivatives with respect to $\ln\eta$. To leading order in the slow roll approximation, note that f^{-2} is simply the power spectrum. The window function, $W(x)$, is given by

$$W(x) = \frac{3\sin(2x)}{2x^3} - \frac{3\cos(2x)}{x^2} - \frac{3\sin(2x)}{2x}. \tag{19}$$

To linear order in the step height c or kinetic energy perturbation $\mathcal{C}$, the power spectrum source is given by $G' = G_0' + G_1'$ with

$$G_1'(\ln\eta) = \tfrac{2}{3}(6\epsilon_1 - 3\eta_1 + \delta_{2,1}), \tag{20}$$

where $G_0'(\ln\eta)$ is the source function in the absence of the step. Compared to η_1 and $\delta_{2,1}$, ϵ_1 is negligible and

$$G_1' \approx -\frac{\mathcal{C}}{6}\left[\left(\frac{\eta}{\eta_f}\right)^3 F'\right]'. \tag{21}$$

We can now evaluate the power spectrum. Inserting Eq. (21) into Eq. (16), integrating by parts and dropping the negligible boundary terms, we obtain

$$\ln\Delta^2_{\mathcal{R}}(k) = \ln\Delta^2_{\mathcal{R},0}(k) + \frac{\mathcal{C}}{6}\int_{\eta_*}^{\infty}\frac{d\eta}{\eta}W'(k\eta)\left(\frac{\eta}{\eta_f}\right)^3 F'. \tag{22}$$

In the $d \to 0$ limit, F' becomes 2 times a delta function at $\ln\eta_f$, given our convention that the step height is $2c$ and so in this limit

$$\lim_{d\to 0}\ln\Delta^2_{\mathcal{R}}(k) = \ln\Delta^2_{\mathcal{R},0}(k) + \frac{\mathcal{C}}{3}W'(k\eta_f). \tag{23}$$

Notice that since $W'(x) = dW/d\ln x$,

$$W'(x) = \left(-3 + \frac{9}{x^2}\right)\cos 2x + \left(15 - \frac{9}{x^2}\right)\frac{\sin 2x}{2x}, \tag{24}$$

and in this limit there are oscillations of amplitude $\mathcal{C}$ in the power spectrum out to $k \to \infty$. This behavior is reminiscent of the Fourier transform of a function with a sharp feature in real space. In Appendix A, we shall see that this intuition is borne out by an analysis of the real space correlation function and that the high k oscillations correspond to a feature at $r = 2\eta_f$.

As we move away from the $d \to 0$ limit, the function F' has finite width of order $\Delta\eta/\eta_f \sim d/\sqrt{\epsilon_0}$, whereas the oscillatory features in W' are of order $\Delta\eta \sim 1/k$. Therefore the delta function approximation holds for $k\eta_f \ll \sqrt{\epsilon_0}/d$. For larger values, we expect the integral to be smaller due to integration over the oscillations in W'. In other words, the $d \to 0$ results should be multiplied by some damping factor that depends on $k\eta_f d/\sqrt{\epsilon_0}$.

In order to explicitly evaluate this damping function, we now assume the form for F given in Eq. (2). The required integrals then take the form

$$I = \int_{\eta_*}^{\infty} d\ln\eta f(k\eta)\,\mathrm{sech}^2\left[\frac{\sqrt{2\epsilon_0}}{d}\ln\left(\frac{\eta_f}{\eta}\right)\right], \tag{25}$$

where $f(k\eta)$ is a polynomial times a sine or cosine and we take η_* to be a time well after the inflaton has crossed the feature. In the limit that $d \to 0$, the polynomial varies slowly while sech^2 is nonzero, and consequently we can replace it by its value when sech^2 is peaked, namely, $(k\eta)^n \to (k\eta_f)^n$. We are then left to evaluate integrals such as

$$I = \int_{\eta_*}^{\infty} d\ln\eta \sin(2k\eta)\mathrm{sech}^2\left[\frac{\sqrt{2\epsilon_0}}{d}\ln\left(\frac{\eta_f}{\eta}\right)\right], \tag{26}$$

as well as the same thing with sine replaced by cosine. Working in the limit $\eta_* \to 0$ and changing variable to $y = -(\sqrt{2\epsilon_0}/d)\ln(\eta/\eta_f)$, the integral can be written

$$I = \frac{d}{\sqrt{2\epsilon_0}}\int_{-\infty}^{\infty} dy \sin\left[2k\eta_f \exp\left(-\frac{d}{\sqrt{2\epsilon_0}}y\right)\right]\mathrm{sech}^2 y. \tag{27}$$

The integrand above only has support for $y \in (-1, 1)$ and, in the limit $d \to 0$, the phase of the sine varies slowly, and thus we can expand,

$$I \approx \frac{d}{\sqrt{2\epsilon_0}}\int_{-\infty}^{\infty} dy \sin\left[2k\eta_f\left(1 - \frac{d}{\sqrt{2\epsilon_0}}y\right)\right]\mathrm{sech}^2 y. \tag{28}$$

The phase error of the expression in brackets is $\mathcal{O}(k\eta_f(yd/\sqrt{2\epsilon_0})^2)$ and, given the support, the approximation is valid for $k\eta_f \ll 2\pi\epsilon_0/d^2$. But, since $d/\sqrt{2\epsilon_0} \ll 1$, this only breaks down for values of $k\eta_f$ that have many oscillations in the region $(-1, 1)$ and are hence far into the region where the integral is already negligible. The integral in Eq. (28) can then be performed by integrating around the square contour in the complex plane, with vertices at $(R, 0)$, $(R, i\pi)$, $(-R, i\pi)$, and $(-R, 0)$ and taking the limit $R \to \infty$, obtaining

$$I \approx 2\frac{d}{\sqrt{2\epsilon_0}}\mathcal{D}\left(\frac{k\eta_f}{x_d}\right)\sin(2k\eta_f), \tag{29}$$

and similarly for the terms with $\cos(2k\eta_f)$. Here

$$x_d = \frac{\sqrt{2\epsilon_0}}{\pi d} \tag{30}$$

determines the value of $k\eta_f$ at which damping starts to become important and

$$\mathcal{D}(y) = \frac{y}{\sinh y} \tag{31}$$

is the damping envelope for the tanh step profile.

Generically then, the power spectrum takes the form

$$\ln\Delta^2_{\mathcal{R}}(k) = \ln\Delta^2_{\mathcal{R},0}(k) + \frac{\mathcal{C}}{3}\mathcal{D}\left(\frac{k\eta_f}{x_d}\right)W'(k\eta_f). \tag{32}$$

Here, the oscillating window function W' is modulated by the decaying envelope $\mathcal{D}$ which is set by the details of the step. As $x \to 0$, $W'(x) \to 0$, and no spurious superhorizon contributions during inflation are generated. Interestingly, the amplitude of the perturbation is independent of the width of the step, while the range (in k space) in which the perturbation persists is independent of the height of the step. This analytic solution was derived in a different way by Stewart [18] who also noted that different functions F simply change the damping envelope. Similar conclusions were also reached in connection with steps arising from features due to duality cascades in brane inflation [19]. In

Appendix A, we address the paradox that even if the feature scale η_f is greater than the current horizon, the power spectrum can retain oscillations to arbitrarily high k.

B. Numerical comparison and nonlinear scaling

In Figs. 1–3, we compare this approximation to the exact solution. We choose a model with $V_0 = m^2\phi^2/2$, and show curves for $d = 0.01$ in Fig. 1 and $d = 0.001$ in Fig. 2, to illustrate the damping behavior. We summarize the other parameters used in Table I.

For $c = 10^{-5} \ll \epsilon_0/6$ (see Figs. 1 and 2), the agreement is excellent both in the amplitude and phase of the results. With $c = 10^{-5}$ the inflaton crosses ϕ_f at $\eta = 1454.6$ Mpc, which agrees to 0.1% with $\eta_f = 1456.1$ Mpc, defined as the epoch when the inflaton crosses the feature for no step $c = 0$. In the lower panels of Figs. 1 and 2 we plot the difference between our analytic approximation in Eq. (32) and a numerical evaluation of the spectrum. The error on our approximation here is at the level of 5%, and is contained in a component that is out of phase by $\pi/2$ with our approximation. As we point out in Appendix B, this error can be attributed to slow roll corrections to the mode functions which are not captured by our leading order approximation at Eq. (16). Furthermore, the spectra also disagree on the percent level on scales far from the $k \sim 1/\eta_f$. This disagreement is due to our analytic approximation of Eq. (16) by Eq. (32) and can be corrected in a straightforward manner by including subleading terms in the power spectrum source, G', at Eq. (21).

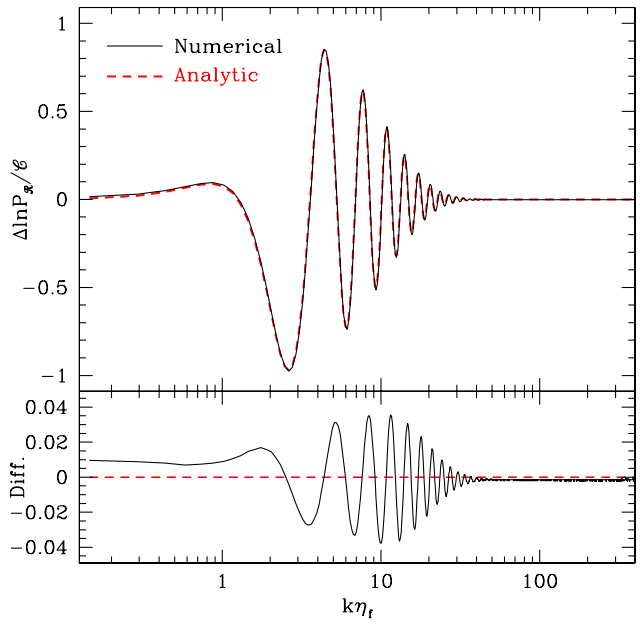

FIG. 1 (color online). Initial curvature power spectrum evaluated numerically (black solid curves) compared with using the approximation in Eq. (32) (dashed red curves) for a small amplitude step $c = 10^{-5} \ll \epsilon_0/6$ (or $\mathcal{C} \ll 1$), where the approximation is expected to work, and a step width, $d = 10^{-2}$, or $x_d \approx 4.3$. The lower panel shows the difference between the two curves, numerical minus analytic. The remaining parameters used in both models are shown in Table I.

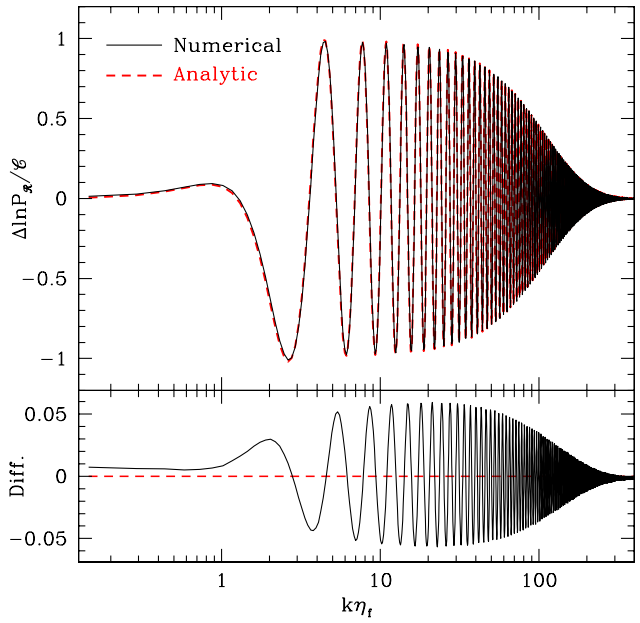

FIG. 2 (color online). Same as Fig. 1 but using a smaller value of the step width. Here we take $d = 10^{-3}$, or $x_d \approx 43$.

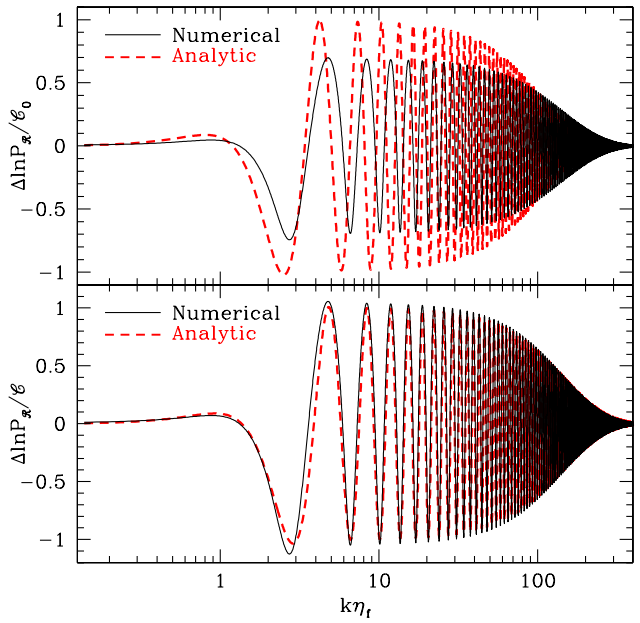

FIG. 3 (color online). Initial curvature power spectrum evaluated numerically (solid black curves) compared with the approximation in Eq. (32) (dashed red curves) for a large amplitude $c = \epsilon_0/6$ (or $\mathcal{C}_0 = 1$, $\mathcal{C} = 2/3$), where the linear expansion is violated by order unity terms. Using the leading order expressions for the step location, oscillation amplitude, and damping η_f, $\mathcal{C} = \mathcal{C}_0$, and x_d (upper panel) leads to phase and amplitude errors that are largely corrected by nonlinearly rescaling these parameters using Eqs. (33) and (35) (lower panel).

TABLE I. Fiducial model parameters for a step at ϕ_f on a potential $V_0 = m^2\phi^2/2$ with physical baryon and cold dark matter densities $\Omega_b h^2$, $\Omega_c h^2$, 100 times the angular size of the sound horizon θ, and the optical depth to reionization τ.

Parameter	Value
m	7.126×10^{-6}
ϕ_f	14.668
ϵ_0	0.009 25
$100\Omega_b h^2$	2.231
$\Omega_c h^2$	0.114
θ	1.040 1
τ	0.084

For $c = \epsilon_0/6$ (see Fig. 3, upper panel), we see both an error in the amplitude, especially at the first few oscillations, as well as a difference in phase. As discussed in the previous section, the phase error simply represents a difference between when the inflaton crosses the feature at ϕ_f relative to the $c = 0$ model. Here the inflaton crosses the feature at $\eta = 1271.7$ Mpc. If we instead define η_f in the analytic expression Eq. (32) to be

$$\eta_f \equiv \eta(\phi_f), \tag{33}$$

we eliminate the phase error. We can also substantially improve the fit by rescaling of the value of ϵ_0 to include the first order perturbation as the field crosses the step,

$$\epsilon_H(\eta_f) \approx \epsilon_0 + 3c. \tag{34}$$

Note that the first order expression suffices since its accuracy is guaranteed by energy conservation so long as $c \ll 1$. In particular, we can define the nonlinear amplitude and damping as

$$\mathcal{C} \equiv \frac{6c}{\epsilon_0 + 3c}, \qquad x_d \equiv \frac{\sqrt{2\epsilon_0 + 6c}}{\pi d}. \tag{35}$$

We demonstrate these nonlinear corrections with the general form of Eq. (32) in the lower panel of Fig. 3. The parameter $\mathcal{C}$ in the lower panel is related to the original linearized version $\mathcal{C}_0 = 6c/\epsilon_0$ in the upper panel by

$$\mathcal{C} = \frac{\mathcal{C}_0}{1 + \mathcal{C}_0/2}. \tag{36}$$

We employ these definitions of η_f, $\mathcal{C}$, and x_d from this point forward. In Table II, we compile a guide to the step parameter notation used in the rest of this paper.

TABLE II. Step parameters and their defining equations.

Parameter	Definition	Eq.
F	Step shape function	(1)
ϕ_f	Potential step position	(1)
η_f	Step crossing time	(33)
c	Potential step height	(1)
$\mathcal{C}$	Kinetic energy perturbation	(35)
$\mathcal{C}_0$	Linearized $\mathcal{C}$	(36)
A_C	Angular power spectrum amplitude	(69)
A_B	Angular bispectrum amplitude	(94)
d	Potential step width	(1)
x_d	Dimensionless damping scale	(35)
ℓ_d	Angular damping multipole	(95)
$\mathcal{D}$	Damping function	(31)

IV. CURVATURE BISPECTRUM

In Sec. IV A we briefly describe the method we use to calculate the bispectrum. For more detail, we refer the reader to [17,20,21]. We use this method to derive an analytic approximation in Sec. IV B. In Sec. IV C, we discuss limiting cases and consistency checks for the approximation and in Sec. IV D we compare it with direct numerical computation of the exact solution.

A. The action and the in-in formalism

In this paper to move beyond the linear equations of motion, we work in comoving gauge in which the time slicing is chosen so that the inflaton is unperturbed. In this gauge the scalar degree of freedom is the comoving curvature perturbation, while the remaining physical metric degrees of freedom are the two polarizations of the transverse traceless tensor perturbation. Tensor perturbations are not enhanced due to the presence of the step [22] and thus we neglect them here. We make use of the interaction picture, where we choose our basis so that the fields diagonalize the Hamiltonian arising from the quadratic action,

$$S_2 = \frac{1}{2}\int dt d^3x a^3 2\epsilon_H \left[\dot{\mathcal{R}}^2 - \frac{(\partial\mathcal{R})^2}{a^2}\right]. \tag{37}$$

In this picture the Hamiltonian arising from cubic and higher order terms in the Lagrangian, which we shall refer to as the interaction Hamiltonian, H_I, evolves the states. At leading order, the tree-level bispectrum at time t_* is then given by [20]

$$\langle \hat{\mathcal{R}}_{\mathbf{k}_1}(t_*)\hat{\mathcal{R}}_{\mathbf{k}_2}(t_*)\hat{\mathcal{R}}_{\mathbf{k}_3}(t_*)\rangle = 2\mathrm{Re}\left[-i\int_{-\infty}^{t_*} dt \langle \hat{\mathcal{R}}_{\mathbf{k}_1}(t_*)\hat{\mathcal{R}}_{\mathbf{k}_2}(t_*)\hat{\mathcal{R}}_{\mathbf{k}_3}(t_*)H_I(t)\rangle\right]. \tag{38}$$

At leading order in fluctuations, the interaction Hamiltonian in Eq. (38) arises from the cubic action. In this work we are interested in potentials in which the inflaton undergoes a sharp transient acceleration but inflation is not interrupted. Consequently, $\epsilon_H \ll 1$ everywhere and, to a very good approximation, the cubic action is given by

$$S_3 \approx \int dt d^3x \Big[a^3 \epsilon_H (\dot{\epsilon}_H - \dot{\eta}_H) \mathcal{R}^2 \dot{\mathcal{R}} - \frac{d}{dt}(a^3 \epsilon_H (\epsilon_H - \eta_H) \mathcal{R}^2 \dot{\mathcal{R}}) \Big]. \quad (39)$$

Note that, after switching to conformal time, $\eta = \int_t^{t_{\rm end}} dt'/a(t)$ (defined to be positive during inflation), and performing some integration by parts, the action in Eq. (39) can be written as

$$S_3 = \int d^3x d\eta 2a^2 \epsilon_H (\eta_H - \epsilon_H) \mathcal{R} [\mathcal{R}'^2 - (\partial \mathcal{R})^2] \quad (40)$$

and thus (for this interaction),

$$\mathcal{L}_3 = 2(\eta_H - \epsilon_H) \mathcal{R} \mathcal{L}_2. \quad (41)$$

Naively, in order that we trust our perturbative evaluation of correlation functions using the interaction picture, we might demand that $\mathcal{L}_3 < \mathcal{L}_2$ so that the evolution of the operators is well described by the equations of motion arising from the quadratic action. Thus we require at least

$$2(\eta_H - \epsilon_H) \mathcal{R} < 1. \quad (42)$$

We shall see that in the context of the step model, this constraint places a lower limit on the step width d that we can consider using perturbative techniques.

In conformal time, the relevant interaction Hamiltonian that follows from the action in Eq. (39) is given by

$$H_I(\eta) = -\int \frac{d^3q_a}{(2\pi)^3} \frac{d^3q_b}{(2\pi)^3} \frac{d^3q_c}{(2\pi)^3} (2\pi)^3 \delta^3(\mathbf{q}_a + \mathbf{q}_b + \mathbf{q}_c) \times \Big[\frac{a^2 \epsilon_H}{3\eta^2} (\epsilon_H - \eta_H)' (\hat{\mathcal{R}}_{\mathbf{q}_a} \hat{\mathcal{R}}_{\mathbf{q}_b} \hat{\mathcal{R}}_{\mathbf{q}_c})' - \frac{d}{d\eta} \Big(\frac{a^2 \epsilon_H}{3\eta} (\epsilon_H - \eta_H) (\hat{\mathcal{R}}_{\mathbf{q}_a} \hat{\mathcal{R}}_{\mathbf{q}_b} \hat{\mathcal{R}}_{\mathbf{q}_c})' \Big) \Big], \quad (43)$$

where recall $' \equiv d/d\ln\eta$. In this expression, the fields $\mathcal{R}$ are interaction picture fields chosen to diagonalize the Hamiltonian derived from the quadratic action in Eq. (37).

We define the bispectrum through

$$\langle \hat{\mathcal{R}}_{\mathbf{k}_1} \hat{\mathcal{R}}_{\mathbf{k}_2} \hat{\mathcal{R}}_{\mathbf{k}_3} \rangle = (2\pi)^3 \delta(\mathbf{k}_1 + \mathbf{k}_2 + \mathbf{k}_3) B_{\mathcal{R}}(k_1, k_2, k_3), \quad (44)$$

where

$$B_{\mathcal{R}}(k_1, k_2, k_3) = 4{\rm Re} \Big\{ i \mathcal{R}_{k_1}(\eta_*) \mathcal{R}_{k_2}(\eta_*) \mathcal{R}_{k_3}(\eta_*) \times \Big[\int_{\eta_*}^{\infty} \frac{d\eta}{\eta^2} a^2 \epsilon_H (\epsilon_H - \eta_H)' (\mathcal{R}^*_{k_1} \mathcal{R}^*_{k_2} \mathcal{R}^*_{k_3})' + \frac{a^2 \epsilon_H}{\eta_*} (\epsilon_H - \eta_H) (\mathcal{R}^*_{k_1} \mathcal{R}^*_{k_2} \mathcal{R}^*_{k_3})'|_{\eta=\eta_*} \Big] \Big\}, \quad (45)$$

and Re denotes the real part. We choose η_* to be a time well after the inflaton has crossed the feature, and $\epsilon_1 = \eta_1 = \delta_{2,1} = 0$. Consequently, the second term in Eq. (45) is tiny, and we neglect it in what follows. The derivation of Eq. (45) is described in detail in [17], and we refer the reader to this work for details.

B. Analytic bispectrum solutions

As described in [17], the GSR approach proceeds by iteratively correcting the evolution of the mode function for the effect of deviations from de Sitter space. As we will see in this section, in the limit in which $d \to 0$ the mode functions, $\mathcal{R}_k$, are well treated as unperturbed, and the non-Gaussian features are well described by integrals involving only the unperturbed mode functions. We have already seen that, even in the limit $d \to 0$, the power spectrum, which may be thought of as the square modulus of the mode functions, gains a correction that is $\mathcal{O}(c/\epsilon_H)$. Thus at linear order, the corrections involving the perturbed mode functions will be small compared to those arising from the perturbed slow roll parameters.

There is an additional weak constraint on d from Eq. (42) due to the perturbative expansion. The perturbations in the curvature themselves do not become large as the field crosses the feature, and thus we may approximate $\mathcal{R} \sim 10^{-5}$. Since ϵ_H remains small, we can neglect it and focus on η_H. Near the step, from above, we know that

$$\eta_H = \frac{\ddot{\phi}}{H^2 \dot{\phi}} \sim \frac{c}{\sqrt{\epsilon_0}} \frac{1}{d}. \quad (46)$$

Thus, with $\epsilon_0 \sim 0.01$, this implies the limit on the ratio

$$\frac{c}{d} < 10^4. \quad (47)$$

In the limit of infinitesimal width $d \to 0$ with finite height, while the field fluctuations remain small, they are no longer well characterized by their tree level N-point functions. On the other hand, this is not a particularly restrictive constraint and when considering the impact on the primary CMB anisotropy is equivalent to taking $d \to 0$. Nevertheless, it does cure the weak logarithmic divergence in the real space correlation function discussed in Appendix A.

In the GSR approach, as described in detail in [17], we can approximate Eq. (45) for the bispectrum as

$$B_{\mathcal{R}}(k_1, k_2, k_3) \approx \frac{(2\pi)^4}{k_1^3 k_2^3 k_3^3} \frac{\Delta_{\mathcal{R}}(k_1) \Delta_{\mathcal{R}}(k_2) \Delta_{\mathcal{R}}(k_3)}{4} \times \Big[-I_0(K) k_1 k_2 k_3 - I_1(K) \sum_{i \neq j} k_i^2 k_j + I_2(K) K (k_1^2 + k_2^2 + k_3^2) \Big], \quad (48)$$

where $K = k_1 + k_2 + k_3$ is the perimeter of the triangle in momentum space. The principle advantage of Eq. (48) is that it involves integrals universal in K,

$$I_n(K) = G_B(\ln\eta_*)W_n(0) + \int_{\eta_*}^{\infty}\frac{d\eta}{\eta}G_B'(\ln\eta)W_n(K\eta), \tag{49}$$

where

$$W_0(x) = x\sin x, \qquad W_1(x) = \cos x, \qquad W_2(x) = \frac{\sin x}{x}, \tag{50}$$

and the bispectrum source is given by

$$G_B = \left(\frac{\epsilon_H - \eta_H}{f}\right). \tag{51}$$

The function $\Delta_{\mathcal{R}}(k)$ is given by the root of the power spectrum, $\Delta_{\mathcal{R}}(k) = \sqrt{\Delta^2_{\mathcal{R}}(k)}$.

We have already obtained analytic solutions for the power spectrum $\Delta_{\mathcal{R}}(k)$ above, and it remains to evaluate the integrals I_0, I_1, and I_2. Following the analysis for the power spectrum, we split the bispectrum source into a background piece and feature piece, but here the background piece generates a negligible bispectrum. Likewise the boundary term in Eq. (49) is negligible and the ϵ_H term in the source is suppressed by a factor of ϵ_0 in its contribution. Integrating twice by parts, we then obtain from Eq. (14)

$$I_n(K) = \frac{\mathcal{C}}{4f_0}\int_{\eta_*}^{\infty}\frac{d\eta}{\eta}(F-1)\left(\frac{\eta}{\eta_f}\right)^3 W_n''. \tag{52}$$

We can bring this into the form of Eq. (22) with one more integration by parts that defines a new window function

$$X_n(K\eta) = -\int_0^{\eta}\frac{d\tilde{\eta}}{\tilde{\eta}}\left(\frac{\tilde{\eta}}{\eta_f}\right)^3 W_n''(K\tilde{\eta}). \tag{53}$$

Using the approximation for the tanh step in Eq. (29) we obtain

$$I_n(K) = \frac{\mathcal{C}}{2f_0}\mathcal{D}\left(\frac{K\eta_f}{2x_d}\right)X_n(K\eta_f), \tag{54}$$

where recall x_d was defined in Eq. (30) such that $x_d \to \infty$ as $d \to 0$. Explicitly

$$\begin{aligned} X_0(x) &= -\frac{(x^4 - 9x^2 + 54)\cos x}{x^2} + \frac{(2x^4 - 27x^2 + 54)\sin x}{x^3}, \\ X_1(x) &= \frac{3(x^2-6)\cos x}{x^2} + \frac{(x^2-6)(x^2-3)\sin x}{x^3}, \\ X_2(x) &= -\frac{(x^2-9)\cos x}{x^2} + \frac{(4x^2-9)\sin x}{x^3}. \end{aligned} \tag{55}$$

All of these window functions vanish as x^2 as $x \to 0$, which means that we do not generate any spurious superhorizon effects. Notice also that X_0 diverges as x^2 for large x while X_1 diverges linearly and X_3 approaches a constant in this limit. This implies that in the limit $d \to 0$ the quantity in brackets in Eq. (48) increases without bound as $k \to \infty$. For small but finite d, we can estimate the location and height of the peak non-Gaussianity. In this limit the bispectrum is dominated by the quadratic term I_0,

$$I_0 \sim (K\eta_f)^2\frac{\mathcal{C}}{2f_0}\mathcal{D}\left(\frac{K\eta_f}{2x_d}\right)\cos(K\eta_f), \tag{56}$$

whose envelope behaves as $x^3\exp(-x)$ near its peak $x = 3$ or

$$K_{\rm peak} = 6\frac{x_d}{\eta_f}. \tag{57}$$

For a fixed step position, i.e. a fixed value of η_f, as $d \to 0$, the peak of the reduced bispectrum moves to larger and larger values of K. Simultaneously reducing the width of the feature and moving it to larger scales, i.e. increasing η_f, fixes the position of the peak of the reduced bispectrum, while increasing its amplitude proportional to the square of the ratio of step positions and increasing the frequency of its oscillations. Thus the sharper the feature, the larger the non-Gaussianity as anticipated in [19,23,24].

Indeed naively, it might seem that the non-Gaussianity strongly diverges with decreasing d due to the high k modes. Here one must be careful in defining what is meant by a large non-Gaussianity. Note that the bispectrum itself, i.e. the amplitude of individual triangles in k space, does not diverge. It is only when written in terms of the reduced bispectrum or effective $f_{\rm NL}$ that the apparent quadratic divergence appears

$$\frac{6}{5}f_{\rm NL}(k_1,k_2,k_3) \equiv \frac{B_{\mathcal{R}}(k_1,k_2,k_3)}{P_{\mathcal{R}}(k_1)P_{\mathcal{R}}(k_2) + \text{perm}}, \tag{58}$$

where "perm" refers to cyclic permutation of the indices. To see where this arises, we can rewrite the reduced bispectrum in terms of the quantity defined by [12,13]

$$\begin{aligned} \frac{\mathcal{G}(k_1,k_2,k_3)}{k_1k_2k_3} &= \frac{k_1^2k_2^2k_3^2}{(2\pi)^4\tilde{A}_s^2}B_{\mathcal{R}}(k_1,k_2,k_3) \\ &\approx \frac{1}{4}\left(\frac{k_1^3+k_2^3+k_3^3}{k_1k_2k_3}\right)\frac{6}{5}f_{\rm NL}(k_1,k_2,k_3), \end{aligned} \tag{59}$$

where $\tilde{A}_s$ is a constant taken to be $\tilde{A}_s = \Delta^2_{\mathcal{R}}$ for nearly scale invariant spectra. The extra factors of k account for the volume factors in k space or equivalently the number of k-space triangles available. Divergence in the reduced bispectrum is usually associated with an equivalent divergence in the non-Gaussianity by assuming that the individual triangles add coherently. For oscillatory bispectra, counting triangles through k factors leads to a misleading

sense of both the UV divergence and the observability of the non-Gaussianity.

A direct means of seeing this fallacy is to evaluate the non-Gaussianity in the real space three-point correlation function. We show in Appendix A that, similar to the power spectrum oscillations, the oscillating and diverging reduced bispectrum is associated with sharp features in the three-point correlation on scales $r \sim \eta_f$ whose amplitude diverges no more than logarithmically. The oscillations in the bispectrum prevent triangles from coherently adding up to a large non-Gaussianity in real space. Furthermore we have seen that there is a mild limitation on our derivation of $c/d < 10^4$ from the validity of the perturbative expansion of the action which prevents even the logarithmic divergence from being manifest.

C. Squeezed limit

It is well known that the bispectrum of curvature fluctuations produced by a single scalar field during inflation satisfies a consistency relation which relates the bispectrum in the squeezed limit to the slope of the power spectrum [20,25]. Since we have analytic solutions for both the bispectrum and power spectrum, this provides us with a nontrivial test of our results.

In the limit where one of the momenta is much smaller than the other two, $k_S \ll k_L$, the consistency relation implies for the reduced bispectrum

$$\frac{6}{5} f_{\rm NL}(k_{\rm S}, k_{\rm L}, k_{\rm L}) = -\frac{1}{2}\frac{d\ln\Delta^2_{\mathcal{R}}}{d\ln k}\bigg|_{k_{\rm L}} \approx 2\frac{\mathcal{G}(k_{\rm S}, k_{\rm L}, k_{\rm L})}{k_{\rm L}^3}, \tag{60}$$

where the approximation holds for nearly scale invariant power spectra. Equation (48) then implies that, in this limit,

$$\frac{d\ln\Delta^2_{\mathcal{R}}}{d\ln k}\bigg|_{k_{\rm L}} = f_0[2I_1 - 4I_2]_{K=2k_{\rm L}}. \tag{61}$$

Now, from Eq. (32), and dropping terms of order $\mathcal{O}(d/\sqrt{2\epsilon_0})$—which amounts to ignoring the variation of the envelope function—we find

$$\frac{d\ln\Delta^2_{\mathcal{R}}}{d\ln k}\bigg|_{k_{\rm L}} = n_s(k_{\rm L}) - 1 + \frac{\mathcal{C}}{3}\mathcal{D}\left(\frac{k\eta_f}{x_d}\right)W''(k\eta_f). \tag{62}$$

Comparing Eq. (62) to Eq. (61) using Eq. (55), and ignoring the slow roll suppressed terms, we find that in this approximation, the consistency relation is satisfied.

A second nontrivial check of our results is that corrections to the squeezed limit of the bispectrum in Eq. (48) are proportional to $(k_{\rm S}/k_{\rm L})^2$, where $k_{\rm S}$ is the side that is being taken to zero. This is in accordance with the behavior of the so-called "not so squeezed limit" [26].

D. Numerical comparison

We begin with a comparison for a small step amplitude. In Fig. 4 we plot the bispectrum resulting from a step with height $c = 10^{-5}$ and width $d = 0.001$. We show the result of evaluating Eq. (45) numerically as well as the result of using the analytic approximation in Eq. (48). Overall, in both amplitude and frequency the approximation is excellent. We show a more detailed comparison in the lower panel, where we divide the difference by the envelope of the analytic expectation

$$\frac{9}{8}\frac{\Delta^3_{\mathcal{R},0}(k)}{\tilde{A}_S^{3/2}}(k\eta_f)^2\mathcal{D}\left(\frac{3k\eta_f}{2x_d}\right), \tag{63}$$

where the amplitude of the power spectrum is taken throughout this section to be $\tilde{A}_S = 2.45 \times 10^{-9}$. The good overall agreement hides an oscillatory 10% residual error.

Given that we are perturbing in $\mathcal{C} \sim 0.6\%$ here, this cannot be an $\mathcal{O}(\mathcal{C}^2)$ correction. In Appendix B, we demonstrate that these corrections are largely due to slow roll corrections to the mode functions. On superhorizon scales, these corrections lead to a phase shift in the growing mode of the curvature perturbation, resulting in a correction on

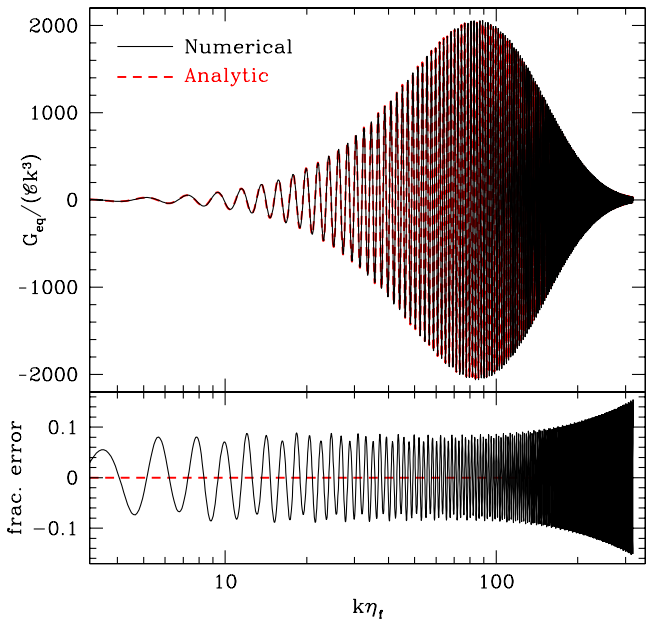

FIG. 4 (color online). Equilateral bispectrum computed using the analytic approximation in Eq. (48) (red dashed curves) compared with a full numerical evaluation of the integral in Eq. (45) for a small amplitude $c = 10^{-5}$ (or $\mathcal{C} \ll 1$). The lower panel shows the difference between the curves, expressed as a fraction of the envelope of the analytic approximation in Eq. (63).

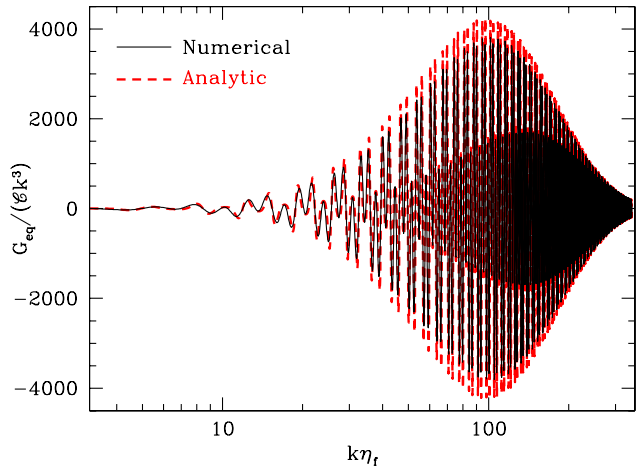

FIG. 5 (color online). Equilateral bispectrum computed using the analytic approximation in Eq. (48) (red dashed curves) compared with a full numerical evaluation of the integral in Eq. (45) for a large amplitude $c \approx \epsilon_0/6$ (or $\mathcal{C}_0 = 1$, $\mathcal{C} = 2/3$). Here the location, amplitude, and damping scale of the feature have been nonlinearly scaled according to Eqs. (33) and (35).

the 10% level to the bispectrum. In fact, as pointed out by [27], leading order slow roll corrections generically lead to 10% rather than $\mathcal{O}(\epsilon_0) \sim 1\%$ corrections as one might naively guess. Additionally, note that the error begins to increase for modes that are far into the damping window. These momenta have many oscillations during the period where the bispectrum source in Eq. (49) is nonzero and are thus in the region where our approximation in Eq. (29) is beginning to break down. Given that this is occurring in the region where the bispectrum is strongly damped, it will have little effect on our results.

As we increase the step height, the leading order approximation for η_f, $\mathcal{C}$, and x_d in Eq. (53) breaks down. Just as in the power spectrum, these errors in phase and amplitude are largely corrected by the nonlinear rescalings of Eqs. (33) and (35) as shown in Fig. 5. While residual errors of 20%–40% remain, they are largely contained in a $\pi/2$ out of phase component rather than in an overall amplitude error, and are related to the nonlinear analog of the corrections discussed in Appendix B. Furthermore, the modulation of the oscillations comes from the power spectrum prefactors of the analytic expression causing the inner and outer envelope effects seen in Fig. 5. In the signal-to-noise calculation that follows, such a modulation mainly cancels out and in fact the use of the simple unmodulated $\mathcal{C} \to 0$ form of $\mathcal{G}/\mathcal{C}$ in Fig. 4 suffices out to $\mathcal{C} \sim 1$ for our purposes.

V. CMB POWER SPECTRUM

In Sec. V A we discuss the phenomenology of a sharp step in the inflaton potential on the CMB temperature power spectrum and derive scaling relations based on projection effects. We then consider WMAP constraints on the location and height of the step in Sec. V B.

A. Scaling relations

The oscillatory features in the curvature power spectrum transfer onto the temperature anisotropy spectrum in a manner that reflects projection onto the recombination surface, evolution through the acoustically oscillating plasma, and gravitational lensing after recombination. These same effects impact the angular bispectrum as well and so it is useful to obtain some physical intuition in the simpler case of the power spectrum.

Projection effects damp the amplitude of the k-space oscillations for modes where $k\eta_f \gg 1$. It is simple to derive scaling relations for this effect in the flat-sky approximation. Ignoring for the moment the acoustic evolution by taking the Sachs-Wolfe limit, the temperature field $a(\hat{\mathbf{n}}) = \Delta T/T$, in the angular direction $\hat{\mathbf{n}}$, is given by

$$a(\hat{\mathbf{n}}) = -\frac{1}{5}\mathcal{R}(\mathbf{x} = D\hat{\mathbf{n}}) = -\frac{1}{5}\int \frac{d^3k}{(2\pi)^3}\mathcal{R}_{\mathbf{k}}e^{i\mathbf{k}\cdot D\hat{\mathbf{n}}}, \tag{64}$$

where D is the distance to recombination. The power spectrum then becomes

$$C_\ell = \frac{1}{5^2D^2}\int \frac{dk_\parallel}{2\pi}P_{\mathcal{R}}(\mathbf{k} = (\boldsymbol{l}/D, k_\parallel)), \tag{65}$$

where $\parallel$ is the direction along the line of sight, orthogonal to the plane of the sky.

Taking the $k\eta_f \gg 1$ and $d \to 0$ limits of the change to the power spectrum in Eq. (32) and assuming $\Delta^2_{\mathcal{R},0} \approx$ const so that

$$C_{\ell,0} = \frac{2\pi}{\ell^2}\frac{\Delta^2_{\mathcal{R},0}}{5^2}, \tag{66}$$

the fractional change in the power spectrum is given by

$$\frac{\Delta C_\ell}{C_\ell} \approx -\mathcal{C}P\left(\frac{2\ell\eta_f}{D}\right) \tag{67}$$

with the projection factor

$$P(x) = \int_1^\infty \frac{dz}{z^2}\frac{1}{\sqrt{z^2-1}}\cos(xz) \approx \sqrt{\frac{\pi}{2x}}\cos(x + \pi/4), \tag{68}$$

where the approximation is in the $x \gg 1$ or $\ell \gg D/2\eta_f$ limit and can be proven by considering that $d^2P/dx^2 = (\pi/2)Y_0(x)$. Rapid oscillations in k space are therefore suppressed in ℓ space by a factor of $(\ell/\ell_f)^{-1/2}$ where $\ell_f = D/\eta_f$. It is useful then to scale the numerical results to this expectation by defining the scaling factor

$$A_C = \mathcal{C}\left(\frac{\eta_f}{1\ \mathrm{Gpc}}\right)^{-1/2}. \tag{69}$$

Note that dividing out by the factor of A_C appropriately rescales the oscillations to be order unity at low ℓ and damp as $\ell^{-1/2}$ according to the envelope

$$\sqrt{\frac{\pi}{2}}\left(\frac{\ell}{D/(1\ \mathrm{Gpc})}\right)^{-1/2}. \tag{70}$$

In Fig. 6 we show a comparison between the full numerical result and these expectations for a model with $V_0 = m^2\phi^2/2$, and parameters defined in Table I. With this model, $\eta_f = 1.44$ Gpc and $D = 14.18$ Gpc. We take for illustrative purposes $c = 10^{-5}$ and $d = 10^{-5}$.

There are two notable differences between the full result vs the flat-sky Sachs-Wolfe scaling. The first is that the oscillations are modulated by the acoustic transfer. This reflects the fact that at nodes in the acoustic oscillations between the acoustic peaks there is no transfer of power to local temperature fluctuations. The second notable effect is a stronger damping starting at $\ell \sim 10^3$. This is due to gravitational lensing as demonstrated in Fig. 6. Without lensing the envelope follows the $\ell^{-1/2}$ scaling of Eq. (70) as expected. For this reason, when considering the bispectrum where lensing effects are more difficult to calculate, we will always take an $\ell_{\mathrm{max}} = 2000$ where lensing effects become order unity for the power spectrum oscillations.

It is also interesting to explore the scaling with the feature scale η_f. For a model with features at the WMAP power spectrum glitches $\eta_f \approx 1.44$ Gpc. For changes by a factor of a few around this value, the results scale as expected as shown in Fig. 7. However, as the feature scale approaches the distance to recombination, projection effects take on a very different character. As discussed in Appendix A, sky curvature prevents a superhorizon feature scale from leaving any imprint on the CMB.

For this reason, when considering the bispectrum where we calculate in the flat-sky approximation, we restrict ourselves to $\eta_f \lesssim 10$ Gpc.

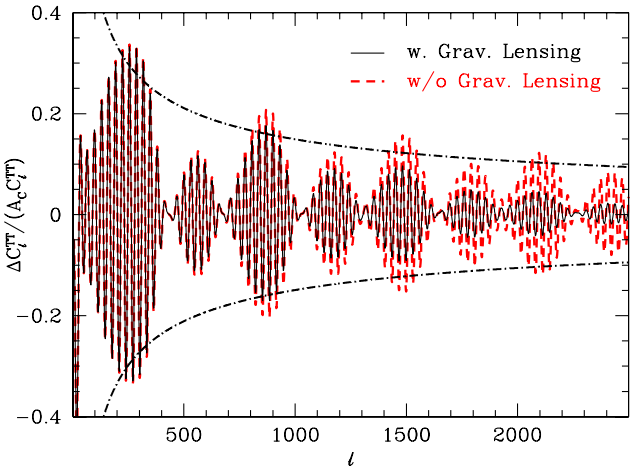

FIG. 6 (color online). Fractional difference of the temperature power spectrum of a model with $\eta_f = 1.44$ Gpc, $c = 10^{-5}$, and $d = 10^{-5}$, relative to a model with $c = 0$ per unit power spectrum feature amplitude A_C [see Eq. (69)]. The case without gravitational lensing is shown by red dashed lines, and when gravitational lensing is taken into account is shown by black solid lines. In black dot-dashed lines we show the expected $\ell^{-1/2}$ envelope from Eq. (70).

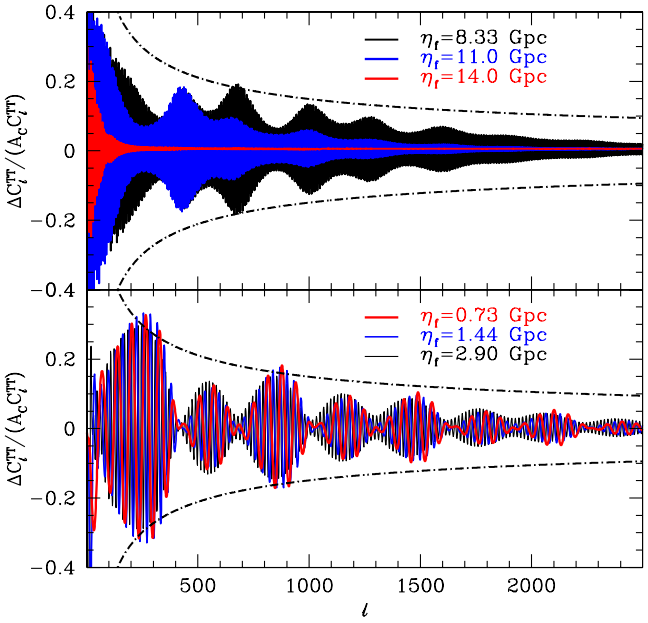

FIG. 7 (color online). Fractional difference of the temperature power spectrum (relative to a model with $c = 0$) of a model with $c = 10^{-5}$ and $d = 10^{-5}$ and different step positions. Gravitational lensing is taken into account in these examples. Note that as $D/\eta_f \to 1$ (in the upper panel), the nodes shift, and the shape changes significantly. In black dot-dashed lines we show the expected $\ell^{-1/2}$ envelope from Eq. (70).

B. Constraints

The WMAP7 temperature and polarization power spectra place constraints on the height, width, and location of a step in the inflaton potential. These constraints then limit the observability of corresponding features in the bispectrum. In order to limit models to reasonable cosmologies we also add the following data sets: BICEP and QUAD, which include polarization constraints [28,29], UNION [30] supernovae data, the SHOES measurement of $H_0 = (74.2 \pm 3.6)$ km/s/Mpc [31], and a big bang nucleosynthesis constraint of $\Omega_b h^2 = 0.022 \pm 0.002$ [32]. We include the effect of gravitational lensing on the CMB.

With these data sets and their likelihood functions, we perform a Markov chain Monte Carlo (MCMC) likelihood analysis on the joint step and cosmological parameters. We parametrize the initial curvature power spectrum as

$$\ln\Delta^2_{\mathcal{R}}(k) = \ln A_s + (n_s - 1)\ln\left(\frac{k}{0.05\ \mathrm{Mpc}^{-1}}\right) + \frac{A_C}{3}\left(\frac{\eta_f}{1\ \mathrm{Gpc}}\right)^{1/2}\mathcal{D}\left(\frac{k\eta_f}{x_d}\right)W'(k\eta_f). \quad (71)$$

Since we are interested in the $x_d \to \infty$ limit, we take a sufficiently small width d in which the damping behavior falls outside of the WMAP range of observation. The initial conditions are then described by 4 parameters $\{A_s, n_s, A_C, \ln\eta_f\}$, to which we add 4 cosmological parameters $\{\Omega_b h^2, \Omega_c h^2, \theta, \tau\}$ in a flat ΛCDM context. We use A_C as the normalization parameter since we expect its errors to be roughly independent of η_f.

We take flat priors on each of these 8 parameters. For all but $\ln\eta_f$ the prior range is an uninformative $>45\sigma$ of the posterior in each. We start with a coarse analysis in a wide range in $0.4 < \eta_f/\mathrm{Gpc} < 12$. Errors on A_C throughout the whole range are approximately $\sigma(A_C) \sim 0.03$–0.06, consistent with the scaling arguments above, but for certain discrete ranges of η_f there is a preference for nonzero mean values. These multiple maxima make a global MCMC analysis highly inefficient.

In Fig. 8, we instead show the result of separate MCMC chains at fixed values of η_f away from these special regions at widely separated $\eta_f = 1.44$, and 11 Gpc. The results here are consistent with $A_C = 0$ and yield 1-sided 95% confidence level bounds of $A_C < 0.05$, 0.10, respectively.

Around specific values of η_f a model with $A_C \approx 0.1$ is actually a better fit to the data than $A_C = 0$. In Fig. 8, we show an example with $\eta_f = 8.1$ Gpc. Preference for high frequency oscillations in the power spectrum around the first acoustic peak in the WMAP data have previously been noted by Ref. [33] and more recently by Refs. [34,35] in different contexts. In Fig. 9, we plot an example from the 2D chain. Here $\eta_f = 8.163$ Gpc and $A_C = 0.11$. Note that this model improves the total likelihood by $2\Delta\ln L = 11.5$ for the two extra parameters. Moreover, this improvement comes from the WMAP likelihood with $2\Delta\ln L_{\mathrm{WMAP}} = 11.6$. Importantly, it does not come from the low multipole moments nor the glitches at $\ell = 20$–40 but mainly oscillations with a period of $\Delta\ell \approx 5.4$ around the first acoustic peak $100 \le \ell \le 300$ with contributions continuing out to the beam scale. Small variations in η_f around this value also produce similar improvements as long as the angular scale η_f/D remains fixed via allowed adjustments of other cosmological parameters, mainly $\Omega_m h^2$.

Other specific values of η_f show comparable likelihood improvements, for example, at $\eta_f = 5.135$ Gpc and $A_C = 0.09$, $2\Delta\ln L = 9.9$. While this level of improvement for 2 parameters is notable, it is possible that it represents fitting of excess noise at the few percent level in C_ℓ that is not well modeled in the likelihood function.

If these improvements are in fact signal and not noise, then there are sharp predictions that can be verified with future data. We shall see in the next section that the bispectrum is observably large so long as the oscillations

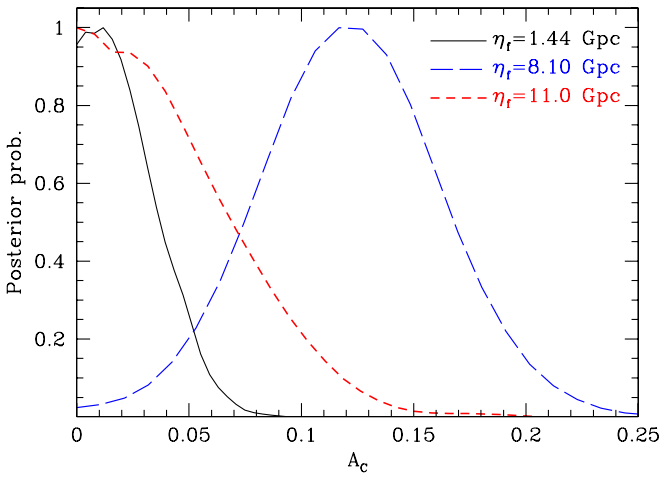

FIG. 8 (color online). Posterior probability distribution of the oscillation amplitude A_C in the angular power spectrum for representative value of $\eta_f = 1.44$, 8.1, and 11 Gpc. The constraint weakens as η_f approaches the horizon for typical cases. For $\eta_f \sim 8.1$ Gpc and other specific values, the peak of the posterior is shifted to $A_C \sim 0.1$ with comparable distribution width.

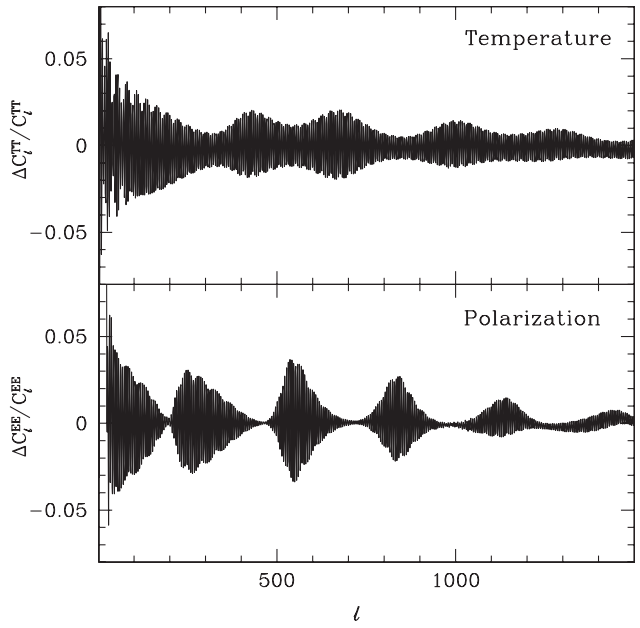

FIG. 9. Fractional angular power spectrum differences between the maximum likelihood sharp-step model ($A_C = 0.11$, $\eta_f = 8.163$ Gpc) and pure power law model ($A_C = 0$). The WMAP data prefer a few percent oscillation in the temperature power spectrum (top panel) around the first acoustic peak by $2\Delta\ln L = 11.6$. This model predicts matching E-polarization power spectrum oscillations (bottom panel) modulated by an orthogonal acoustic phase.

persist undamped to $\ell \gtrsim 500$. Furthermore there must be matching features in the polarization power spectra (see Fig. 9). The oscillations in the polarization power spectra are comparable but larger at the peak as they are less affected by projection and modulated by an orthogonal acoustic transfer. Detection of this matching signal in polarization would make a convincing case for a primordial origin of the improvement.

VI. CMB BISPECTRUM

We can now use our analytic results to estimate the signal-to-noise ratio (SNR) in the bispectrum. We review the SNR calculation for a cosmic variance limited data set in Sec. VI A and approximate methods for its estimation in Sec. VI B. From this approximate method, we derive scaling relations for its dependence on the amplitude, width, and location of the step feature in Sec. VI C and calibrate them against numerical calculations in Sec. VI D.

A. Cosmic variance

The temperature or angular bispectrum is defined as the three-point function of the spherical harmonic coefficients $a_{\ell m}$ of the temperature anisotropy

$$B_{\ell_1\ell_2\ell_3} = \sum_{m_1 m_2 m_3} \begin{pmatrix} \ell_1 & \ell_2 & \ell_3 \\ m_1 & m_2 & m_3 \end{pmatrix} \langle a_{\ell_1 m_1} a_{\ell_2 m_2} a_{\ell_3 m_3} \rangle. \quad (72)$$

The cosmic variance of the Gaussian part of the field puts an irreducible limit on the SNR of

$$\left(\frac{S}{N}\right)^2 = \sum_{\ell_3 \geq \ell_2 \geq \ell_1} \frac{B^2_{\ell_1\ell_2\ell_3}}{C_{\ell_1} C_{\ell_2} C_{\ell_3} d_{\ell_1\ell_2\ell_3}}, \quad (73)$$

where

$$d_{\ell_1\ell_2\ell_3} = [1 + \delta_{\ell_1\ell_2} + \delta_{\ell_2\ell_3} + \delta_{\ell_3\ell_1} + 2\delta_{\ell_1\ell_2}\delta_{\ell_2\ell_3}], \quad (74)$$

accounts for permuted contractions of repeated ℓ's and the angular power spectrum is defined by

$$\langle a^*_{\ell m} a_{\ell' m'} \rangle = \delta_{\ell\ell'}\delta_{mm'} C_\ell. \quad (75)$$

We thus require an efficient means of predicting the angular bispectrum given the curvature bispectrum.

The bispectrum arising from the approximations in Eqs. (29) and (48) looks especially formidable to project onto the angular sky due to the inseparable damping function $\mathcal{D}(x)$. In Appendix C, we demonstrate that, to a good approximation, this bispectrum can be cast into an approximately separable form, which will make the full projection onto the angular sky a much more tractable problem. Still, this separable form requires computational intensive operations making an exploration of the whole parameter space difficult. We leave evaluation of this to future work.

B. Approximations

Here we are interested only in an order of magnitude estimate for the SNR through a crude computation of the angular bispectrum from the curvature bispectrum. We therefore take the flat-sky approach and the Sachs-Wolfe limit for the temperature anisotropy.

In the flat-sky approximation, the angular bispectrum is defined by the three-point function of the Fourier moments of the temperature field given by $a(\mathbf{l})$

$$\langle a(\mathbf{l}_1) a(\mathbf{l}_2) a(\mathbf{l}_3) \rangle = (2\pi)^2 \delta(\mathbf{l}_1 + \mathbf{l}_2 + \mathbf{l}_3) B_{(\ell_1,\ell_2,\ell_3)}. \quad (76)$$

For $\ell_1, \ell_2, \ell_3 \gg 1$, it is related to the all-sky bispectra as [36]

$$B_{\ell_1\ell_2\ell_3} = \sqrt{\frac{(2\ell_1+1)(2\ell_2+1)(2\ell_3+1)}{4\pi}} \times \begin{pmatrix} \ell_1 & \ell_2 & \ell_3 \\ 0 & 0 & 0 \end{pmatrix} B_{(\ell_1,\ell_2,\ell_3)}. \quad (77)$$

Under the flat Sachs-Wolfe approximation of Eq. (64), the bispectrum becomes

$$B_{(\ell_1,\ell_2,\ell_3)} = -\frac{2}{5^3 D^4} \int_0^\infty \frac{dk_{1||}}{2\pi} \int_{-\infty}^\infty \frac{dk_{2||}}{2\pi} B_{\mathcal{R}}(k_1, k_2, k_3), \quad (78)$$

where

$$\mathbf{k}_1 = (\mathbf{l}_1/D, k_{1||}), \quad \mathbf{k}_2 = (\mathbf{l}_2/D, k_{2||}), \quad \mathbf{k}_3 = -\mathbf{k}_1 - \mathbf{k}_2. \quad (79)$$

It is useful to note that with the correspondence between all-sky and flat-sky expressions [36]

$$\left(\frac{S}{N}\right)^2 \approx 4\pi \int \frac{d^2\ell_1}{(2\pi)^2} \int \frac{d^2\ell_2}{(2\pi)^2} \frac{B^2_{(\ell_1,\ell_2,\ell_3)}}{6 C_{\ell_1} C_{\ell_2} C_{\ell_3}}. \quad (80)$$

Scaling relations for the SNR can thus be derived from scaling relationships for the flat-sky spectra combined with a counting of triangles in the available phase space.

C. Scaling arguments

Before we numerically compute Eq. (73), we can estimate how strongly we expect the SNR to scale as we add triangles.

1. Local bispectrum

As a proof of technique, let us first examine the case of a local non-Gaussianity where the reduced bispectrum is a constant or

$$B_{\mathcal{R}}(k_1, k_2, k_3) = \tfrac{6}{5} f_{\rm NL} [P_{\mathcal{R}}(k_1) P_{\mathcal{R}}(k_2) + \text{perm}]. \quad (81)$$

The signal is dominated by squeezed configurations $\ell_S \ll \ell_L$ and the above arguments imply that

$$B^{\rm local}_{(\ell_S,\ell_L,\ell_L)} \propto \frac{\Delta^2_{\mathcal{R}}(\ell_L/D)\Delta^2_{\mathcal{R}}(\ell_S/D)}{\ell^2_L\ell^2_S}. \quad (82)$$

Consequently, the SNR for triangles with long and short sides between $\ell_{\rm min}$ and $\ell_{\rm max}$ for a scale invariant power spectrum will go as

$$\left(\frac{S}{N}\right)^2 \propto \int d^2\ell_S \int d^2\ell_L \frac{\ell^4_L\ell^2_S}{\ell^4_L\ell^4_S} \propto \ell^2_{\rm max}\ln\left(\frac{\ell_{\rm max}}{\ell_{\rm min}}\right), \quad (83)$$

where we have used Eq. (66) to take $C_\ell \propto \ell^{-2}$ in the same flat-sky, Sachs-Wolfe limit.

The integrals can be thought of as counting triangles: There are ℓ^2_L ways of choosing one of the long sides of the triangles and likewise ℓ^2_S ways of choosing the short side. The final long side is determined by requiring the triangle close and so the total number of triangles becomes $\ell^2_L\ell^2_S$.

The naively infrared divergent integral is regulated by the lowest multipole available, which in our cosmic variance limited calculation is $\ell_{\rm min} = 2$. This leaves an overall scaling of $\ell^2_{\rm max}$, in agreement with the cosmic variance limit of a well-known result in the literature that the error on $f_{\rm NL}$ drops as $N^{-1/2}_{\rm pix}$, where $N_{\rm pix} = f_{\rm sky}\ell^2_{\rm max}$ is the number of observed pixels [37,38].

2. Feature bispectrum

We can now look at our feature bispectrum. There are now three cases we need to consider, the SNR being dominated by contributions from

(1) equilateral type shapes: $k_1 \sim k_2 \sim k_3$;
(2) flat type shapes: $k_1 \sim k_2 \sim 2k_3$; and
(3) squeezed type shapes, as in the local case $k_3 \ll k_1 \sim k_2$.

We consider these separately below, estimating how their contribution to the SNR scales with the number of modes.

Equilateral type.—Consider the leading contribution to the bispectrum of Eq. (48) assuming a scale invariant spectrum, and taking $f^{-1}_0 = \Delta_{\mathcal{R}}(k)$. In the UV or large-$k$ limit, the bispectrum is dominated by the term quadratic in the perimeter of the momentum triangle

$$B_{\mathcal{R}}(k_1,k_2,k_3) \approx \frac{\mathcal{C}}{2}(2\pi)^4\frac{\Delta^4_{\mathcal{R}}}{4}\mathcal{D}\left(\frac{K\eta_f}{2x_d}\right) \times\left[\frac{1}{(k_1k_2k_3)^2}(K\eta_f)^2\cos(K\eta_f)\right]. \quad (84)$$

The effect of the damping envelope $\mathcal{D}(x)$ is to impose a limit on the maximum scale that can contribute to the SNR, $\ell_{\rm max}$. Neglecting the prefactors and taking $\ell_f = D/\eta_f$, we expect the projection of the bispectrum in Eq. (84) onto the flat sky to scale as

$$B_{(\ell,\ell,\ell)} \propto \frac{1}{\ell^4}\left(\frac{\ell}{\ell_f}\right) = \ell^{-1}_f\ell^{-3}, \quad (85)$$

where the $(K\eta_f)^2$ supplies two factors of (ℓ/ℓ_f) and the two integrals over $k_{||}$ suppress the result by $(\ell/\ell_f)^{-1}$ due to the oscillatory integrands as in the power spectrum. Finally, the integrals over ℓ_1 and ℓ_2 provide a factor of $\ell^4_{\rm max}$ and yield

$$\left(\frac{S}{N}\right)^2_{\rm eq} \propto \ell^4_{\rm max}\frac{\ell^{-2}_f\ell^{-6}_{\rm max}}{\ell^{-6}_{\rm max}} \propto \frac{\ell^4_{\rm max}}{\ell^2_f}. \quad (86)$$

The $\ell^4_{\rm max}$ factor can be thought of as a counting of equilateral type triangles: In three dimensions, there are $\ell^2_{\rm max}$ ways to choose the first side, another $\ell^2_{\rm max}$ ways to choose the second side, while the third side is determined by requiring the triangle close, yielding $\sim\ell^4_{\rm max}$ triangles.

Flat type.—Flat triangles scale equivalently to equilateral type triangles,

$$B_{(\ell,\ell,2\ell)} \propto \ell^{-1}_f\ell^{-3}, \quad (87)$$

however, due to the restriction that all modes be colinear, this reduces the number of triangles available. Flat triangles correspond to the restriction $|\ell_1 - \ell_2 - \ell_3| < \Delta L$, where $L = \ell_1 + \ell_2 + \ell_3$ and ΔL is the tolerance. With this restriction, we expect the number of triangles to scale as $\ell^4_{\rm max}\sqrt{\Delta L/\ell_{\rm max}}$. The curved sky imposes a minimum $\Delta L = 1$, and thus we expect the number of triangles to scale as $\ell^{3.5}_{\rm max}$ and the contribution of flat triangles to the SNR scales as

$$\left(\frac{S}{N}\right)^2_{\rm flat} \propto \ell^{3.5}_{\rm max}\frac{\ell^{-2}_f\ell^{-6}_{\rm max}}{\ell^{-6}_{\rm max}} \sim \ell^{-2}_f\ell^{3.5}_{\rm max}. \quad (88)$$

Thus flat triangles contribute less to the total SNR than equilateral triangles for $\ell_{\rm max} \gg \ell_f$.

Squeezed type.—Considering now squeezed triangles, in the limit $k_S \ll k_L$, and taking the leading order term

$$B_{\mathcal{R}}(k_L,k_L,k_S) \approx -\frac{\mathcal{C}}{2}(2\pi)^4\frac{\Delta^4_{\mathcal{R}}}{4}\mathcal{D}\left(\frac{k_L\eta_f}{x_d}\right)2k_L\eta_f \times\sin(2k_L\eta_f)k^{-3}_Lk^{-3}_S, \quad (89)$$

we estimate that this bispectrum contributes to the signal in squeezed angular space configurations $\ell_S \ll \ell_L$ as

$$B_{(\ell_S,\ell_L,\ell_L)} \propto \ell^{-5/2}_S\ell^{-3/2}_L. \quad (90)$$

Compared to the result in Eq. (85), for a fixed ℓ_S, the signal in squeezed triangles falls slower in the UV relative to the signal in equilateral triangles. However, considering the SNR,

$$\left(\frac{S}{N}\right)^2_{\rm sq} \propto \int d^2\ell_S\int d^2\ell_L\ell_L\ell^{-3}_S, \quad (91)$$

we obtain

$$\left(\frac{S}{N}\right)^2 \propto \frac{\ell^3_{\rm max}}{\ell_{\rm min}}, \quad (92)$$

which implies that the contribution of squeezed triangles compared to the equilateral type goes to zero as $\ell_{\rm max} \to \infty$. Interestingly, while squeezed triangles dominate the signal at high ℓ, they do not dominate the signal to noise. The reason for this is twofold. Squeezed triangles in themselves suffer from higher cosmic variance which, for a given triangle, eliminates the scaling advantage. In addition, there are many less triangles which contribute to the squeezed limit.

D. Scaling and numerical results

To summarize the scaling relations of the previous section, for small values of $\mathcal{C}$,

$$\left(\frac{S}{N}\right)^2 \propto \mathcal{C}^2 \frac{\ell_{\rm max}^4}{\ell_f^2} = \mathcal{C}^2 \frac{\ell_{\rm max}^4 \eta_f^2}{D^2}, \tag{93}$$

as $d \to 0$ and for $\ell_{\rm max} \gg \ell_f$. With this behavior in mind, we define the angular bispectrum amplitude,

$$A_B = \mathcal{C}\left(\frac{\eta_f}{1\ {\rm Gpc}}\right) = \frac{6c}{\epsilon_0 + 3c}\left(\frac{\eta_f}{1\ {\rm Gpc}}\right) = A_C\left(\frac{\eta_f}{1\ {\rm Gpc}}\right)^{3/2}, \tag{94}$$

which takes into account the dependence of the amplitude on the step scale, η_f. Compared with A_C the analogous amplitude for the angular power spectrum, the bispectrum amplitude increases as $\eta_f^{3/2}$. Recalling that the observational errors on A_C are only weakly dependent on η_f, the SNR is maximized by placing the feature at the largest observable scales, near the current horizon.

With a finite d there is an effective maximum multipole beyond which the SNR saturates. This scale depends on η_f as

$$\ell_d = \frac{2D}{\eta_f} x_d = \frac{2D}{\eta_f} \frac{\sqrt{2\epsilon_0 + 6c}}{\pi d}. \tag{95}$$

In what follows we simply scale out the multipole space bispectrum amplitude A_B, and present the square of the SNR per unit A_B as a function of the multipole space damping scale, ℓ_d or $\ell_{\rm max}$. These redefinitions render our results independent of the choice of the model parameters $\{\phi_f, c, d\}$. Of course to make connection with a particular model, one must rescale by the appropriate factors of A_B and choose the correct damping scale.

We verify the SNR scaling behaviors and obtain the proportionality coefficient in the scaling relations by numerically evaluating Eq. (73). In the upper panel of Fig. 10 we show the contribution to the SNR of all triangles and the contribution from triangles that are exactly flat. The close agreement of ℓ^4 and $\ell^{3.5}$ curves with the numerical results verifies our scaling relations, confirming that the SNR is dominated by triangles whose sides are all of comparable length. For this test, the feature occurs at a scale $\eta_f = 1.44$ Gpc.

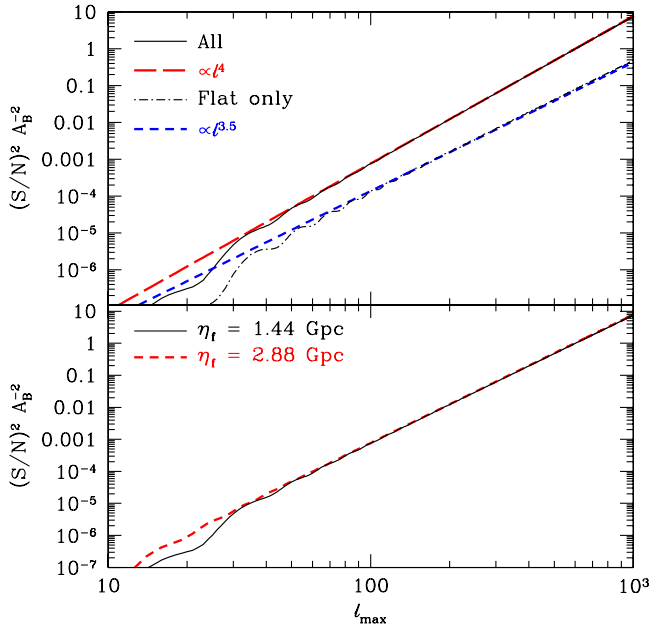

FIG. 10 (color online). The square of the SNR per unit bispectrum amplitude (A_B) for $\ell_d = 8514$ for all triangles, and for flat configurations only. We also plot the scaling relations from Sec. VI C. In the lower panel, we demonstrate that changing η_f while fixing A_B and ℓ_d leaves the SNR fixed at high ℓ.

The lower panel in Fig. 10 demonstrates that our results are independent of the specific choice of η_f; plotted is the square of the SNR per unit bispectrum amplitude under a shift of the feature from 1.44 Gpc (black, solid curve) to 2.88 Gpc (red, dashed curve), while simultaneously reducing the width of the step as to hold the damping scale, ℓ_d, constant.

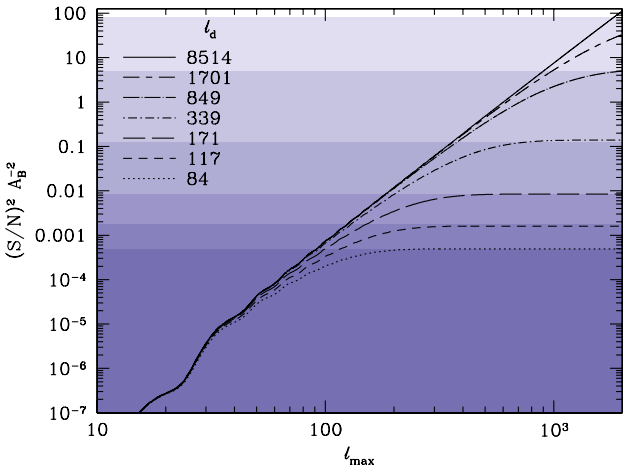

FIG. 11 (color online). The square of the SNR per unit bispectrum amplitude (A_B) for various damping scales ℓ_d. The shaded regions indicate the prediction of our scaling formula in Eq. (96) and match the asymptotic high $\ell \gg \ell_d$ saturation point for each case.

In Fig. 11, we show the dependence of the SNR on the angular damping scale ℓ_d. Notice the SNR saturates once the maximum multipole $\ell_{\rm max}$ exceeds the damping scale. In fact, to excellent approximation, the value at saturation can be approximated from the $d = 0$ results by setting $\ell_{\rm max} = 1.06\ell_d$. However, for values of d where $\ell_d > 2000$ secondary anisotropy contributions such as gravitational lensing and the Sunyaev-Zeldovich effect become important. Furthermore the Planck satellite will be limited by its instrumental beam to lower multipoles.

Thus our rough approximation of the maximal signal to noise accessible to the CMB temperature bispectrum can be expressed in terms of our scaling parameters and the amplitude of the features in the temperature power spectrum as

$$\left(\frac{S}{N}\right)^2 \approx 1.2\left(\frac{A_C}{0.1}\right)^2\left(\frac{\eta_f}{1\ \mathrm{Gpc}}\right)^3\left(\frac{\ell_{\rm max}}{2000}\right)^4, \qquad (96)$$

where $\ell_{\rm max} = \min(1.06\ell_d, 2000)$. Combined with the upper limit of $A_C \lesssim 0.05$ for a typical value of η_f (see Fig. 8), one infers that sharp steps with $\eta_f \gtrsim 2$ Gpc have potentially observable features in the bispectrum while still being consistent with current power spectrum results. For the maximum likelihood model, where $A_C = 0.11$ and $\eta_f = 8.163$ Gpc, the maximal $(S/N)^2 \approx 790$. In fact, even taking $\ell_{\rm max} = 800$, the $(S/N)^2 \approx 20$ and so there may even be information about this model in the WMAP data if an optimal analysis can be performed.

Our scaling relation makes it seem that we can increase the SNR without bound by moving the feature to larger and larger scales. However, just as was the case in the power spectrum, our flat-sky approximation overestimates the bispectrum as η_f approaches the current horizon due to projection effects on the curved sky. Adopting the same maximal scale of $\eta_f < 10$ Gpc as was found for the power spectrum, the SNR can be at most comparable to that of the maximum likelihood model.

Should a horizon scale feature be detected in the data, then one should also consider the sample (co)variance of the finite number of such features that can fit in our horizon volume when measuring the parameters associated with the feature. For upper limits, the Gaussian noise variance suffices.

VII. DISCUSSION

We have investigated the power spectrum and bispectrum of curvature fluctuations generated by a sharp-step feature in the inflationary potential. In the limit where the change in potential energy due to the step is small compared to the kinetic energy of the inflaton, we have demonstrated that the background system can be solved perturbatively in this small parameter.

Using this solution for the background evolution of the inflaton, we obtained closed form, approximate analytic solutions for both the power spectrum and bispectrum of curvature fluctuations. The analytic solutions generically take the form of an oscillating window function times a damping function. The form of the window function is set by the behavior of the step in the infinitely sharp limit with its characteristic frequency determined by the step position in conformal time, η_f. The damping function on the other hand determines the maximal wave number out to which the oscillations persist, which scales with the inverse of the finite width d, with a form factor that depends on the shape of the step. In this work we have explicitly calculated the damping function for a step with a hyperbolic tangent shape.

Our analytic power spectrum and bispectrum solutions pass several important consistency checks. They vanish for modes that are superhorizon size when the field crosses the step, and thus do not introduce spurious superhorizon effects. They satisfy the consistency relation which relates the squeezed limit of the bispectrum to the tilt of the power spectrum, or scalar spectral index. Additionally, leading order corrections to this relationship scale only as the square of the squeezed side. Numerically, for very small perturbations to the kinetic energy, our solutions are accurate to approximately 10%. This difference is largely due to slow roll corrections to the mode functions, which introduce additional phase shifts and thus alter the form of the non-Gaussianity. Somewhat surprisingly, rather than 1% level corrections as one might naively guess, these types of corrections generically lead to 10% corrections to the bispectrum.

As the step height increases, and the perturbation to the kinetic energy becomes large, the analytic solutions begin to break down due to two effects. First, the perturbation to the kinetic energy becomes large and inflation ends at an appreciably different time for a potential with and without the step. This difference corresponds to a change in the matching of inflationary field scales to physical scales and hence a phase shift between the analytic solution and its numerical counterpart. We make use of the approximate time translation invariance of the inflationary background to absorb this phase shift into a redefinition of the conformal time of the unperturbed background. The second effect is that as the kinetic energy perturbation grows to order unity, our analytic solutions attain a larger amplitude while damping away at a faster rate compared with the numerical results. In our analytic solution these properties are controlled by a single parameter, ϵ_H, which effectively measures the ratio of kinetic to potential energy of the inflaton. At leading order, our analytic solution takes into account only the kinetic energy of the inflaton on the background without the step. However, we have shown that the discrepancy between the numerical and analytic results can be substantially improved by including the first order kinetic energy perturbation in ϵ_H.

As the step width becomes infinitely sharp, the high wave number limit of the spectra exhibits some interesting

behavior. We have found that the perturbation to the curvature power spectrum approaches a constant amplitude oscillation, while the reduced bispectrum, or effective nonlinearity, diverges quadratically in the perimeter of the momentum space triangle. The reduced bispectrum or nonlinearity parameter $f_{\rm NL}$ can thus reach 10^4 or more. While one might naively infer a strongly divergent non-Gaussianity on small spatial or angular scales, the real space analogs of the power spectrum and bispectrum, the two- and three-point correlation functions remain tiny for most configurations, in particular, all those involving only small separations. Oscillations largely prevent the various triangle configurations adding up to anything significant: For the most part they simply average to zero. However, for certain configurations, where the separation between points is comparable to the physical scale of the feature, resonance in the integral leads to logarithmically large values of the correlation. High wave number oscillations in the spectra therefore are the result of Fourier transforming a sharp feature in the correlation functions on large scales.

The real space picture of the bispectrum suggests that the k-space triangles are not all independent as they must sum to yield a sharp feature at a fixed, large scale. This covariance of triangles must be accounted for if such a signal in the bispectrum is detected in the future. In principle, one could use our methods to evaluate higher N-point functions which quantify this covariance and that of the power spectrum. Furthermore, they would provide corroborating evidence for a step and are expected to grow even more strongly with the momentum perimeter than the bispectrum considered here.

On the other hand, to assess the detectability of the bispectrum, it is sufficient to compute the SNR where the noise is attributed to Gaussian random fluctuations only. We utilize our analytic bispectrum solutions to assess detectability as a function of the step location, height, and width. For simplicity, we neglect acoustic transfer and the sky curvature, working in the Sachs-Wolfe and flat-sky limits. This oversimplification suffices for our order of magnitude estimate. Under this approximation, the signal-to-noise ratio is dominated by equilateral triangles and scales with the fourth power of the maximum multipole due to resolution or finite width d. These scaling relations allow us to characterize observability as a function of the step parameters.

The SNR is maximized by placing a sharp feature close to the horizon scale. Since the effective nonlinearity grows quadratically with the ratio of the feature scale to the observed wavelength, placing the feature at larger scales means it can grow to a larger amplitude within the window probed by the CMB. The maximum scale at which one can place the feature before it becomes unobservable is the horizon scale for both the power spectrum and bispectrum. In real space, the high-k behavior of either translates to sharp correlation features at separations comparable to the physical scale of the step. Because of causality, an observer confined to a single position cannot measure a correlation across a distance larger than the horizon. Since in the $d \to 0$ limit oscillations in the power spectrum persist even for superhorizon scale features, the momentum space results naively seem problematic. However, as the horizon scale is approached, the frequency of the oscillations in the spectra approach the fundamental spacing of the spherical harmonics, $\Delta\ell = 1$. Thus, as this scale is exceeded, CMB spectra are rendered insensitive to the presence of the feature, except for an unobservable shift in the monopole.

While one might guess that the angular power spectrum of the CMB would place severe restrictions on large, sharp steps due to their oscillations persisting into the strongly constrained $\ell \sim 200$–400 region, in fact the constraints are considerably weaker. There is an additional source of damping when the oscillating features in the momentum space power spectrum are projected onto the sky. Additionally, effects such as gravitational lensing tend to hide the oscillations on very small scales. Curiously, the WMAP power spectrum data are in fact better fit by such a feature than a pure power law spectrum with $2\Delta \ln L \approx 12$ for the 2 extra parameters. While this improvement may be due to fitting excess noise in WMAP, it is formally more significant than a similar fit of the well-known glitch at $\ell = 20$–40 with 3 extra parameters [8,9].

If this improvement is due to a slow roll violating feature such as a step, there are testable consequences in both the polarization power spectrum and the bispectrum. The polarization power spectrum should carry matching oscillations whose amplitude is less affected by projection. The bispectrum would be detectable as long as the oscillations continue undamped to at least $\ell \sim 500$. In this case, the bispectrum may be able to confirm the primordial origin of such a signal.

ACKNOWLEDGMENTS

We thank Andy Albrecht, Xingang Chen, Richard Easther, Raphael Flauger, and Mark Wyman for useful conversations. This work was supported in part by the Kavli Institute for Cosmological Physics at the University of Chicago through Grants NSF No. PHY-0114422 and NSF No. PHY-0551142 and an endowment from the Kavli Foundation and its founder Fred Kavli. C. D. was additionally supported by the Institute for Advanced Study through the NSF Grant No. AST-0807444 and the Raymond and Beverly Sackler Funds. W. H. was additionally supported by the U.S. Department of Energy Contract No. DE-FG02-90ER-40560 and the David and Lucile Packard Foundation.

APPENDIX A: REAL SPACE CORRELATION

Given that the step feature is localized in time, it is interesting to consider the correlation functions, the real

space analogs of the power spectrum and bispectrum. While somewhat orthogonal to the main thrust of the paper, we will see that the real space correlation functions give insight into causality, sample vs noise variance, consistency relation and the perturbative validity of our expansion of the action. In particular, we shall see that the $k \to \infty$ behavior of the power spectrum and bispectrum correspond to sharp features in the real space correlation functions.

This Appendix is organized as follows. In Sec. A 1, we demonstrate that, in the limit in which $d = 0$, the perturbation to the curvature power spectrum leads to a sharp feature in real space, the modes as $k \to \infty$ summing to give a logarithmically divergent derivative at a single point associated with the physical scale at which the feature occurs. In Sec. A 2, we show that, despite attaining a large nonlinearity, $f_{\rm NL}(k)$, the real space analog of the bispectrum remains small everywhere, except in the vicinity special points, associated with the physical scale of the feature, where it becomes large, diverging as $\sim \ln(d)$. This behavior is shown to be due to the fact that the momentum space triangles only coherently add for very special configurations of the spatial points which lead to resonances in the Fourier integrals. In Sec. A 3, we show that at least some of this behavior can be anticipated from the consistency relation, which relates the slope of the two-point correlation function to a certain limit of the three-point correlation function.

1. Two-point correlation

The two-point correlation function is the Fourier transform of the power spectrum

$$\begin{aligned}\xi_{2\mathcal{R}}(\mathbf{r}_1,\mathbf{r}_2) &\equiv \langle \mathcal{R}(\mathbf{r}_1)\mathcal{R}(\mathbf{r}_2)\rangle \\ &= \left[\prod_{i=1}^{2}\int \frac{d^3k_i}{(2\pi)^3} e^{i\mathbf{k}_i\cdot\mathbf{r}_i}\right] P_{\mathcal{R}}(k_1)(2\pi)^3\delta^3(\mathbf{k}_1+\mathbf{k}_2) \\ &= \int \frac{dk}{k}\frac{\sin(kr)}{kr}\Delta^2_{\mathcal{R}}(k), \end{aligned} \tag{A1}$$

where $r = |\mathbf{r}_1 - \mathbf{r}_2|$.

With our analytic calculation for the power spectrum of the step feature in Sec. III we showed that in the limit in which the step width $d \to 0$, the power spectrum correction attains a constant amplitude oscillation which persists to $k \to \infty$. Corresponding to this high frequency behavior, there must be sharp features in the correlation function.

The contribution of the step feature to $\xi(r)$ can be calculated from Eq. (32) as

$$\Delta\xi_{2\mathcal{R}}(r) = \frac{\mathcal{C}}{3}\int \frac{dk}{k}\frac{\sin(kr)}{kr}\mathcal{D}\left(\frac{\pi d}{\sqrt{2\epsilon_0}}k\eta_f\right)W'(k\eta_f). \tag{A2}$$

When $d = 0$, Eq. (A2) can be evaluated analytically, and one obtains

$$\Delta\xi_{2\mathcal{R}}(r) = -\mathcal{C}J(r/2\eta_f), \tag{A3}$$

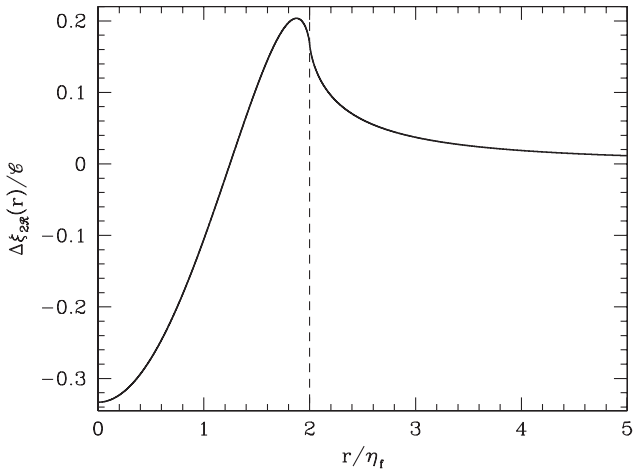

FIG. 12. Real space two-point correlation function changes due to the addition of a step feature ($d \to 0$). At $r/\eta_f = 2$, the slope of the correlation function diverges as the dashed line indicates.

with

$$J(x) = \frac{1}{3} - \frac{x^2}{2} + \frac{x}{2}(x^2-1)\begin{cases}\coth^{-1}x, & x > 1,\\ \tanh^{-1}x, & x < 1.\end{cases} \tag{A4}$$

We plot this function in Fig. 12. In this case, the sum over all of the modes out to infinity results in a sharp feature in the slope at $r = 2\eta_f$ while the function remains finite, and order $\mathcal{O}(\mathcal{C})$ everywhere. The fact that $r = 2\eta_f$ is a special point can in fact be read directly off of the integrand. Since $W' \propto \cos(2k\eta_f)$ at high k and the exponentials in the transform give $\sin(kr)$, contributions from different k modes oscillate away except for the stationary phase point $r = 2\eta_f$. We will use this type of reasoning to deduce the behavior of the three-point function in Sec. A 2 a.

The slope of the correlation function $\xi_{2\mathcal{R}}(r)$ formally diverges for $d = 0$ at the point $r = 2\eta_f$. More generally

$$\begin{aligned}\frac{d\Delta\xi_{2\mathcal{R}}}{d\ln r} = \frac{\mathcal{C}}{3}\Delta^2_{\mathcal{R},0}\int \frac{dk}{k}\left(\cos(kr) - \frac{\sin(kr)}{kr}\right) \\ \times \mathcal{D}\left(\frac{\pi d}{\sqrt{2\epsilon_0}}k\eta_f\right)W'(k\eta_f).\end{aligned} \tag{A5}$$

Given that the damping envelope supplies a $k_{\rm max} \propto d^{-1}$, for $k_{\rm min}\eta_f \gg 1$

$$\frac{d\Delta\xi_{2\mathcal{R}}}{d\ln r} \propto \int_{k_{\rm min}}^{k_{\rm max}} \frac{dk}{k}\cos(kr)\cos(2k\eta_f), \tag{A6}$$

and this integral is logarithmically divergent with d at $r = 2\eta_f$. We will relate this divergence to the bispectrum behavior in Sec. A 3.

Examination of Figs. 1 and 2 also raises an interesting question about causality. As we have demonstrated, a sharp feature in the inflationary potential gives rise to oscillating features in the power spectrum of curvature fluctuations

and as the step becomes sharper and sharper, the oscillating features ring to larger and larger wave numbers, k, before decaying. One might then be tempted to conclude that an observer who only had access to a region of space $\eta < \eta_f$ could measure superhorizon perturbations, by observing oscillations in his power spectra on small scales.

We have, however, also shown that, in real space, these modes simply sum up to a sharp feature at the physical scale corresponding to the size of the physical horizon when the inflaton crosses the feature. One therefore comes to the conclusion that an observer who has access to only a region of space $\eta \ll \eta_f$ cannot measure the feature. The resolution to this apparent discrepancy is that the k-space features are spaced by less than $1/\eta$ and so cannot be sampled in the finite volume. In the CMB this is imposed by the finite volume within the distance to recombination. In a large scale structure, this is similarly imposed by the finite survey volume.

More specifically, in the case of the CMB the projection of these oscillations onto the angular sky imposes a very physical cutoff on the frequency of the oscillations, corresponding to the fundamental spacing of the multipoles, $\Delta\ell = 1$. Oscillations in the power spectrum with a frequency spacing smaller than this fundamental are rendered unobservable when projected onto the spherical sky. In the Sachs-Wolfe approximation,

$$\frac{\ell(\ell+1)C_\ell}{2\pi} = \frac{1}{5^2}\int \frac{dk}{k} j_\ell^2(kD)\Delta^2_{\mathcal{R}}(k). \tag{A7}$$

In the example at hand, at $k\eta_f \gg 1$

$$\Delta^2_{\mathcal{R}}(k) \approx \Delta^2_{\mathcal{R},0}(k)[1 - \mathcal{C}\cos(2k\eta_f)]. \tag{A8}$$

Since the Bessel function oscillates only at a frequency kD, if $2\eta_f \gg D$ then the oscillatory piece cancels out of the integral. This cutoff prevents an observer from obtaining information about sharp features on scales larger than their horizon. However, we note that this cutoff is only exactly enforced by the full projection onto the spherical sky. In particular, in the periodic flat-sky approximation despite enforcing a fundamental spacing of $\Delta\ell = 1$, features with oscillations at $\Delta\ell < 1$ can imprint beat frequencies on the remaining modes making $\delta C_\ell/C_\ell \propto (\ell\eta_f/D)^{-1/2}$ as in Eq. (67). Figure 7 verifies that this scaling breaks in the full sky calculation for $\eta_f \gtrsim D$ leaving a suppressed contribution to the anisotropy.

2. Three-point correlation

Similarly, the three-point correlation function is related to the bispectrum by a Fourier transform of its arguments

$$\begin{aligned}\xi_{3\mathcal{R}}(\mathbf{r}_1,\mathbf{r}_2,\mathbf{r}_3) &\equiv \langle \mathcal{R}(\mathbf{r}_1)\mathcal{R}(\mathbf{r}_2)\mathcal{R}(\mathbf{r}_3)\rangle \\ &= \left[\prod_{i=1}^{3}\int \frac{d^3k_i}{(2\pi)^3} e^{i\mathbf{k}_i\cdot\mathbf{r}_i}\right] B_{\mathcal{R}}(k_1,k_2,k_3)(2\pi)^3 \\ &\quad \times \delta^3(\mathbf{k}_1+\mathbf{k}_2+\mathbf{k}_3).\end{aligned} \tag{A9}$$

For a general configuration and the step potential bispectrum, this integral is difficult to compute. As was the case with the two-point function, we can gain insight on its behavior by first studying resonances in the integrand where the phase is stationary. We can then confirm this behavior by explicitly evaluating simple configurations.

a. Resonances

The bispectrum of the step feature as its width $d \to 0$ and the wave numbers $k_i \to \infty$ have oscillatory behavior given by Eq. (56)

$$B_{\mathcal{R}}(k_1,k_2,k_3) \propto \cos[(k_1+k_2+k_3)\eta_f]. \tag{A10}$$

This implies that in the real space correlation function most of the contributions will integrate away except for special resonant points where the frequencies in the transform match those of the bispectrum.

Without loss of generality, we can set $\mathbf{r}_3 = 0$ and integrate out $\mathbf{k}_3$ in Eq. (A9)

$$\xi_{3\mathcal{R}}(\mathbf{r}_1,\mathbf{r}_2,0) = \prod_{i=1}^{2}\int \frac{d^3k_i}{(2\pi)^3} e^{i\mathbf{k}_i\cdot\mathbf{r}_i} B_{\mathcal{R}}(k_1,k_2,k_3), \tag{A11}$$

where k_3 is now defined by the cosine law. The integrals are thus sums of bispectrum triangles defined by the 6-dimensional vector $\mathbf{K} = (\mathbf{k}_1,\mathbf{k}_2)$. In this 6D vector notation, the phase function

$$\begin{aligned}\phi &\equiv \mathbf{k}_1\cdot\mathbf{r}_1 + \mathbf{k}_2\cdot\mathbf{r}_2 \pm (k_1+k_2+k_3)\eta_f \\ &= \mathbf{K}^{\mathrm{T}}\mathbf{R} \pm \left(\sqrt{\mathbf{K}^{\mathrm{T}}\mathbb{1}_1\mathbf{K}} + \sqrt{\mathbf{K}^{\mathrm{T}}\mathbb{1}_2\mathbf{K}} + \sqrt{\mathbf{K}^{\mathrm{T}}\mathbb{U}\mathbf{K}}\right)\eta_f,\end{aligned} \tag{A12}$$

where $\mathbf{R} = (\mathbf{r}_1,\mathbf{r}_2)$ and we have defined

$$\mathbb{1}_1 = \begin{bmatrix} 1_{3\times3} & 0 \\ 0 & 0 \end{bmatrix}, \quad \mathbb{1}_2 = \begin{bmatrix} 0 & 0 \\ 0 & 1_{3\times3} \end{bmatrix}, \quad \mathbb{U} = \begin{bmatrix} 1_{3\times3} & 1_{3\times3} \\ 1_{3\times3} & 1_{3\times3} \end{bmatrix}. \tag{A13}$$

Now, we can look for points where this is stationary with respect to triangle configuration. Setting $d\phi/d\mathbf{K} = 0$, we obtain

$$\mathbf{R} \pm \left(\frac{\mathbb{1}_1\mathbf{K}}{\sqrt{\mathbf{K}^{\mathrm{T}}\mathbb{1}_1\mathbf{K}}} + \frac{\mathbb{1}_2\mathbf{K}}{\sqrt{\mathbf{K}^{\mathrm{T}}\mathbb{1}_2\mathbf{K}}} + \frac{\mathbb{U}\mathbf{K}}{\sqrt{\mathbf{K}^{\mathrm{T}}\mathbb{U}\mathbf{K}}}\right)\eta_f = 0, \tag{A14}$$

which can be written

$$\mathbf{r}_i = \mp\eta_f(\hat{\mathbf{k}}_i - \hat{\mathbf{k}}_3), \tag{A15}$$

where hats denote unit vectors. Note that the real space resonances occur for triangles that are coplanar with the

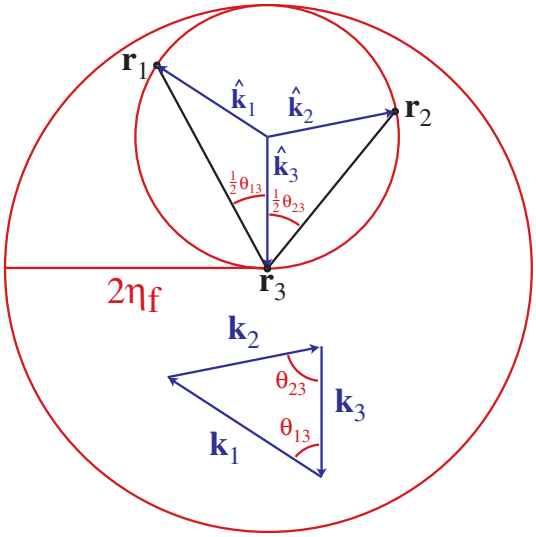

FIG. 13 (color online). Relationship between bispectrum triangle shapes and resonances in the three-point real space correlation function. As $d \to 0$ each set of self-similar bispectrum triangles determined by $(\mathbf{k}_1, \mathbf{k}_2, \mathbf{k}_3)s$, where s is some scale factor, causes a resonance at $(\mathbf{r}_1, \mathbf{r}_2, \mathbf{r}_3)$ and its mirror image. As the overall size of the triangle $s \to \infty$ this resonance becomes sharper and sharper in real space but remains associated with separations $\mathcal{O}(\eta_f)$. Flat triangles are responsible for the largest scale resonance for $\mathbf{r}_1 - \mathbf{r}_3 = \mathbf{r}_2 - \mathbf{r}_3 = 2\eta_f$.

k-space triangles. At these solutions, the phase function reaches

$$\frac{\phi}{\eta_f} = \mp(k_1 + k_2) \pm (\mathbf{k}_1 + \mathbf{k}_2) \cdot \hat{\mathbf{k}}_3 \pm (k_1 + k_2) \pm k_3 = 0, \tag{A16}$$

and so satisfies the constancy condition.

For each k-space triangle geometry there is a resonance in real space triangles that is fixed by the k-space geometry (see Fig. 13). The orientations of $\mathbf{r}_i$ relative to $\mathbf{k}_3$ are determined by the half angles of the respective k-space triangle angles. The physical length r_i varies from a maximum of $2\eta_f$, if $\mathbf{k}_i || -\mathbf{k}_3$; through $\sqrt{2}\eta_f$, if they are orthogonal; to 0, if they are parallel $\mathbf{k}_i || \mathbf{k}_3$. Note, however, that if $r_1 \to 0$ then $r_2 \to 2\eta_f$ so that resonant triangles always have characteristic size η_f. The maximum size of the correlation region of $2\eta_f$ is achieved for flat triangles. Finally, there is no resonance at $\mathbf{r}_1 = \mathbf{r}_2 = \mathbf{r}_3 = 0$ since 3 coparallel k vectors cannot close.

The allowed resonances all correspond to points inscribed on a sphere of radius η_f where rotation in or around the $\mathbf{k}_3$ direction corresponds to a rotation of the real space resonance.

We can also show that these points are extrema rather than unstable saddle points by considering the Hessian

$$H_{ij} = \frac{\partial^2 \phi}{\partial K_i \partial K_j}. \tag{A17}$$

A similar but more tedious exercise shows that this matrix is positive semidefinite. Namely, for any vector $\mathbf{Q} = (\mathbf{q}_1, \mathbf{q}_2)$ defining a direction in the 6-dimensional space of bispectrum triangles with a closure relation $\mathbf{q}_3 = -(\mathbf{q}_1 + \mathbf{q}_2)$

$$\mathbf{Q}^{\mathrm{T}}\mathbf{H}\mathbf{Q} = \sum_{i=1}^{3} \frac{\eta_f}{k_i}[q_i^2 - (\mathbf{q}_i \cdot \hat{\mathbf{k}}_i)^2] \geq 0. \tag{A18}$$

The eigenvalues vanish along the special directions of $\mathbf{q}_i || \mathbf{k}_i$. There are two cases where this happens. The first corresponds to fixing the triangle geometry while changing its overall size. The second is for the family of flat triangles where the sides are all coparallel but the ratio of lengths k_1/k_2 can vary. For these triangles there are two flat directions whereas nondegenerate triangles have only one. Equivalently, Eq. (A16) shows that for both of these cases, the phase function is strictly fixed.

Given the behavior of trajectories in the space of triangles, we can estimate the volume of phase space that satisfies the resonance condition, and thus contributes to the integrals. Except for these special flat directions in the 6-dimensional space, the typical width of the resonances is $\Delta q \sim \sqrt{k/\eta_f}$. Putting this together, we can estimate the degree of convergence or divergence of the three-point correlation function in Eq. (A11). For a typical real space configuration where $\mathbf{r}_1 \neq \mathbf{r}_2$, there is only one flat direction $k_s \sim k_i$ where the triangle size is multiplied by some scale factor s

$$\xi_{3\mathcal{R}}(\mathbf{r}_1, \mathbf{r}_2, 0) \propto \eta_f^2 \int dk_s \left(\frac{k_s}{\eta_f}\right)^{5/2} k_s^{-4} \mathcal{D} \propto \frac{1}{\sqrt{k_{\max}\eta_f}}, \tag{A19}$$

where $k_{\max} \propto d^{-1}$ from the damping function $\mathcal{D}$.

On the other hand, for the special configuration where $\mathbf{r}_1 = \mathbf{r}_2 = 2\eta_f$, there are two flat directions, k_s and $R = k_2/k_1$, which implies the three-point correlation function will scale as

$$\xi_{3\mathcal{R}}(\mathbf{r}_1, \mathbf{r}_2, 0) \propto \eta_f^2 \int k_s dk_s \left(\frac{k_s}{\eta_f}\right)^{2} k_s^{-4} \mathcal{D} \propto \ln(k_{\max}\eta_f), \tag{A20}$$

where we assume that $k_i > \eta_f^{-1}$.

The Hessian also identifies another special case where there is an approximately flat direction if $k_i \ll \eta_f^{-1}$. This is the case of squeezed triangles where one of the sides does not contribute significantly to the phase function. In this case $k_3 \ll k_2 \approx k_1 \equiv k$

$$\phi = \mathbf{k} \cdot (\mathbf{r}_1 - \mathbf{r}_2) \pm 2k\eta_f, \tag{A21}$$

for which the stationary solutions are

$$\mathbf{r}_1 - \mathbf{r}_2 = \pm 2\eta_f \hat{\mathbf{k}}, \tag{A22}$$

such that there is a resonance whenever the separation between any two points is $2\eta_f$, regardless of the position of the third. In this case the dominant term in

the bispectrum goes as $\eta_f k^{-2} k_3^{-3}$ [see Eq. (89)] and the resonance contains one flat direction in $\mathbf{k}$ parallel to $\mathbf{r}_1 - \mathbf{r}_2$ and two orthogonal of width $\sqrt{k/\eta_f}$ each. Therefore the three-point correlation scales as

$$\xi_{3\mathcal{R}}(\mathbf{r}_1, \mathbf{r}_1 + 2\eta_f \hat{\mathbf{e}}, 0) \propto \eta_f \int dk \left(\frac{k}{\eta_f}\right) k^{-2} \mathcal{D} \int d^3k_3 k_3^{-3} \propto \ln(k_{\max}\eta_f) \ln(k_{\min}\eta_f), \quad \text{(A23)}$$

where $\hat{\mathbf{e}}$ is any unit vector. Here the correlation depends on a cutoff in the infrared $k_{\min}$ which in practice comes from the survey volume of the data, i.e. the current horizon for a cosmic variance limited statistic.

These results imply that, despite the naive K^2 divergence of the reduced bispectrum, the three-point correlation at most positions actually converges except if points are separated by $2\eta_f$ where flat and squeezed triangles cause a logarithmic divergence.

The real space picture of the non-Gaussianity of a sharp step raises an interesting question as to the meaning of the noise term in our signal-to-noise calculation. In real space, the increasing $(S/N)^2$ at high k is associated with modes that superimpose to give a sharp correlation feature on large scales. Thus each triangle cannot be considered an independent probe of the non-Gaussianity. By including only the Gaussian contribution to the noise, we neglect this sample covariance of triangles. Our SNR therefore only quantifies detectability of the non-Gaussianity rather than the measurability of parameters associated with the step potential. If in the future, non-Gaussianity of this type is detected, then the covariance must be considered by computing the six-point functions.

b. Configurations

We can test these properties of the three-point function by explicitly evaluating it for a few simple configurations. The expression in Eq. (A9) involve six integrals over a highly oscillatory function, making it difficult to evaluate numerically. However, in the limit in which two of the points are coincident, the expression can be simplified to

$$\xi_{3\mathcal{R}}(r,0,0) = (2\pi)^2 \int \frac{k_1 dk_1}{(2\pi)^3} \int \frac{k_2 dk_2}{(2\pi)^3} \times \int_{|k_1-k_2|}^{k_1+k_2} k_3 dk_3 B_{\mathcal{R}}(k_1,k_2,k_3) \times \left(\frac{\sin(k_1 r)}{k_1 r} + \frac{\sin(k_2 r)}{k_2 r}\right). \quad \text{(A24)}$$

In the limit $d = 0$, using the result for the bispectrum in Sec. IV B, the integral over k_3 in Eq. (A24) can be performed analytically (the result is messy and not particularly enlightening, and we omit it here) leaving a more tractable problem of evaluating only two integrals. In order to numerically evaluate the resulting expression, and render the result at $r/\eta_f = 2$ finite, we need to impose a cutoff in the integral at high wave number. However, the integral needs to be cut off in a way that reflects the fact that triangles of different shapes experience different damping behavior. For nonzero values of d, we note that as long as d is small, this result can be utilized to integrate the bispectrum at finite d, by parts. We then need only keep the boundary term, since the remaining term will be suppressed by a factor of d, and will thus be negligible in the limit $d \to 0$. Moreover, since this explicitly retains the form of the damping function, we automatically apply the correct damping to each shape.

As well as divergences at the point $r/\eta_f = 2$ arising from the ultraviolet parts of the phase space, there are also the usual divergences associated with the infrared parts of the scale invariant power spectra. In reality, these divergences are regulated by the finite size of the longest observable wavelength. To perform the numerical evaluation, we simply apply a hard cutoff on the minimum momenta, $k_{\min}$.

To perform the integration, we write the bispectrum as

$$B_{\mathcal{R}}(k_1,k_2,k_3) \approx \frac{(2\pi)^4}{k_1^3 k_2^3 k_3^3} \frac{\Delta_{\mathcal{R}}(k_1)\Delta_{\mathcal{R}}(k_2)\Delta_{\mathcal{R}}(k_3)}{4} \times \Big[-I_0(K) k_1 k_2 k_3 + I_2(K)(k_1^3 + k_2^3 + k_3^3) + (I_2(K) - I_1(K)) \sum_{i \neq j} k_i^2 k_j \Big]. \quad \text{(A25)}$$

In Fig. 14 we show the contribution to the real space three-point correlation function due to each of the terms in Eq. (A25) at two different values of the step width, or damping scale x_d. In particular, note that the skewness of

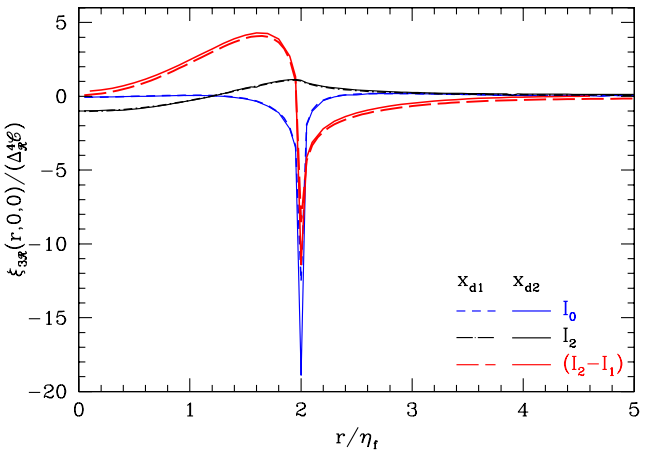

FIG. 14 (color online). Contribution to the real space three-point correlation function from the three terms in Eq. (A25). The thick dashed curves were computed for damping scale $x_d = x_{d1} = 200$ with an infrared cutoff at $k_{\min} = 0.1/\eta_f$, while the corresponding thin solid curves were calculated with $x_{d2} = 1000$.

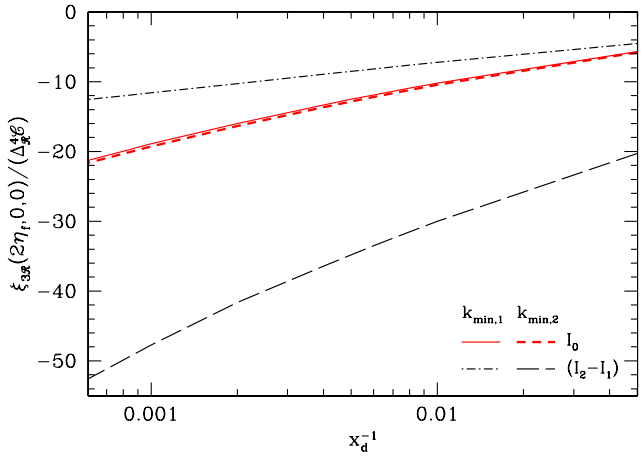

FIG. 15 (color online). Behavior of the various contributions to the real space three-point correlation function $\xi_{3\mathcal{R}}(r,0,0)$ in Eq. (A25) at the point $r = 2\eta_f$ as a function ultraviolet cutoff x_d. The dependence on the infrared cutoff is also demonstrated. Here $k_{\mathrm{min},1} = 0.1/\eta_f$, while $k_{\mathrm{min},2} = 0.001/\eta_f$.

the field is finite, and small while $\xi_{3\mathcal{R}}(r,0,0)$ vanishes quickly for $r/\eta_f > 2$. The three-point function is also largely insensitive to the value of the damping scale, x_d, which regulates the UV, except at the special point, $r = 2\eta_f$, where it diverges. In Fig. 15 we demonstrate that this divergence is no more pathological than $\ln(d)$. Figure 15 also demonstrates the scaling behavior of Eqs. (A20) and (A23); note that the contribution to the three-point function due to the most dominant UV term, I_0, is insensitive to the infrared cutoff, k_{min}, while the term which dominates the squeezed contribution, $I_2 - I_1$, is logarithmically sensitive to the infrared cutoff. The remaining term, in Eq. (A25) is not UV divergent and we omit it from the plot.

All of these properties and scalings are consistent with our resonance estimates from Sec. A 2 a.

3. Real space consistency

To shed light on why the two-point correlation reaches infinite slope at $r = 2\eta_f$ while the three-point correlation logarithmically diverges there, we can extend the familiar k-space consistency relation between the power spectrum and squeezed bispectrum to real space correlation functions.

In fact the k-space consistency argument itself comes from a real space derivation. We follow the analysis of [25] here but make more explicit what is meant by the background. To this end, we split the field up into low pass and high pass filtered pieces

$$\mathcal{R}(\mathbf{x}) = \bar{\mathcal{R}} + \tilde{\mathcal{R}} = \int_{k<k_*} \frac{d^3k}{(2\pi)^3} \mathcal{R}_{\mathbf{k}} e^{i\mathbf{k}\cdot\mathbf{x}} + \int_{k>k_*} \frac{d^3k}{(2\pi)^3} \mathcal{R}_{\mathbf{k}} e^{i\mathbf{k}\cdot\mathbf{x}}. \tag{A26}$$

That is, we split the contributions of the field at each point into contributions from modes shorter than some reference mode k_*, and long wavelength modes assumed to be much longer than this scale. Next we consider the two-point function of the high pass field in the fixed background. Since the background fluctuation is expected to be small, we can functionally expand

$$\langle\tilde{\mathcal{R}}(\mathbf{x}_1)\tilde{\mathcal{R}}(\mathbf{x}_2)\rangle = \langle\tilde{\mathcal{R}}(\mathbf{x}_1)\tilde{\mathcal{R}}(\mathbf{x}_2)\rangle\Big|_{\bar{\mathcal{R}}=0} + \bar{\mathcal{R}}(\mathbf{x}_+) \times \frac{\delta}{\delta\bar{\mathcal{R}}}\langle\tilde{\mathcal{R}}(\mathbf{x}_1)\tilde{\mathcal{R}}(\mathbf{x}_2)\rangle\Big|_{\bar{\mathcal{R}}=0} + \cdots, \tag{A27}$$

where the background field is slowly varying and evaluated in the vicinity of the points, which for definiteness we take to be $\mathbf{x}_+ = (\mathbf{x}_1 + \mathbf{x}_2)/2$. In the presence of the background mode, the metric is

$$ds^2 = -dt^2 + a(t)^2 e^{2\bar{\mathcal{R}}(\mathbf{x})} dx^2. \tag{A28}$$

Then, absorbing the effect of the background mode into a change in variable $\mathbf{x} \to \mathbf{x}' = e^{\bar{\mathcal{R}}(\mathbf{x})}\mathbf{x}$, we induce a change in the separation between points

$$\Delta x \to e^{\bar{\mathcal{R}}(\mathbf{x})}\Delta x. \tag{A29}$$

Defining the two-point correlation function of the high and low pass fields

$$\tilde{\xi}_{2\mathcal{R}}(\Delta x_{12}) = \langle\tilde{\mathcal{R}}(\mathbf{x}_1)\tilde{\mathcal{R}}(\mathbf{x}_2)\rangle|_{\bar{\mathcal{R}}=0} = \int_{k>k_*} \frac{dk}{k} \Delta^2_{\mathcal{R}}(k) \frac{\sin k\Delta x_{12}}{k\Delta x_{12}}, \tag{A30}$$

$$\bar{\xi}_{2\mathcal{R}}(\Delta x_{+3}) = \langle\bar{\mathcal{R}}(\mathbf{x}_+)\bar{\mathcal{R}}(\mathbf{x}_3)\rangle = \int_{k<k_*} \frac{dk}{k} \Delta^2_{\mathcal{R}}(k) \frac{\sin k\Delta x_{+3}}{k\Delta x_{+3}}, \tag{A31}$$

where $\Delta x_{ij} = |\mathbf{x}_i - \mathbf{x}_j|$, we obtain

$$\langle\tilde{\mathcal{R}}(\mathbf{x}_1)\tilde{\mathcal{R}}(\mathbf{x}_2)\rangle = \tilde{\xi}_{2\mathcal{R}}(\Delta x_{12}) + \bar{\mathcal{R}}(\mathbf{x}_+) \frac{d\tilde{\xi}_{2\mathcal{R}}}{d\ln\Delta x_{12}}, \tag{A32}$$

which then correlates with a third point as

$$\langle\tilde{\mathcal{R}}(\mathbf{x}_1)\tilde{\mathcal{R}}(\mathbf{x}_2)\bar{\mathcal{R}}(\mathbf{x}_3)\rangle = \bar{\xi}_{2\mathcal{R}}(\Delta x_{+3}) \frac{d\tilde{\xi}_{2\mathcal{R}}}{d\ln\Delta x_{12}}.$$

This defines the squeezed contribution to the analogous three-point function.

Note that we can Fourier transform this relation to obtain the bispectrum. Given that through integration by parts

$$\frac{d\tilde{\xi}_{2\mathcal{R}}}{d\ln r} = -\int_{k>k_*} \frac{d^3k}{(2\pi)^3} e^{i\mathbf{k}\cdot\mathbf{r}} \left[\frac{1}{k^3} \frac{d(k^3 P_{\mathcal{R}})}{d\ln k}\right], \tag{A33}$$

we obtain immediately

$$B_{\mathcal{R}}(k_1,k_2,k_3) = -P_{\mathcal{R}}(k_3)\left[\frac{1}{k^3} \frac{d(k^3 P_{\mathcal{R}})}{d\ln k}\right]_{k\approx k_1\approx k_2}, \tag{A34}$$

for $k_3 < k_*$, $k_1 \approx k_2 > k_*$ and zero otherwise. This is the well-known Fourier space consistency relation.

Thus we expect the three-point correlation in real space to have a contribution proportional to the slope of the two-point correlation function. For the step potential, the slope of the two-point correlation function at $r = 2\eta_f$ diverges as $\ln k_{\rm max}$, whereas $\bar{\xi}_{2\mathcal{R}}(\Delta x_{+3})$ diverges as $\ln k_{\rm min}$. Thus, with a sufficiently small $k_{\rm min}$, we expect that the three full three-point function will be dominated by these squeezed contributions. Specifically, including the cyclic permutations which account for the pairings of high and low pass filtered fields we expect

$$\xi_{3\mathcal{R}}(r,0,0) \sim -2\ln(k_{\rm min}\eta_f)\Delta^2_{\mathcal{R},0}\frac{d\xi_{2\mathcal{R}}}{d\ln r}, \tag{A35}$$

near $r = 2\eta_f$ for nearly scale invariant spectra taking k_* comparable to but smaller than η_f^{-1}. This explains the scaling of Eq. (A23). In Fig. 16 we demonstrate this relation numerically. Plotted is the contribution to the real space three-point correlation function due to the I_1 and I_2 terms of Eq. (48) and the relation in Eq. (A35). We take $k_{\rm min}$ to be a factor of 10^3 smaller than the feature scale. The agreement is only approximate; however, this is possibly due to the fact that we have not omitted the contribution of nonsqueezed triangles to $\xi_{3\mathcal{R}}$.

The $\ln k_{\rm min}$ divergence is the usual IR divergence of a scale invariant spectrum and is cured in any physical observable by the finite size of the Hubble radius today. The UV divergence from the slope of the two-point function at $r = 2\eta_f$, however weak, signals a breakdown of perturbation theory. In the consistency relation context, the assumed change in the two-point correlation in response to the background mode in Eq. (A27) exceeds the total change in the two-point correlation as a function of r.

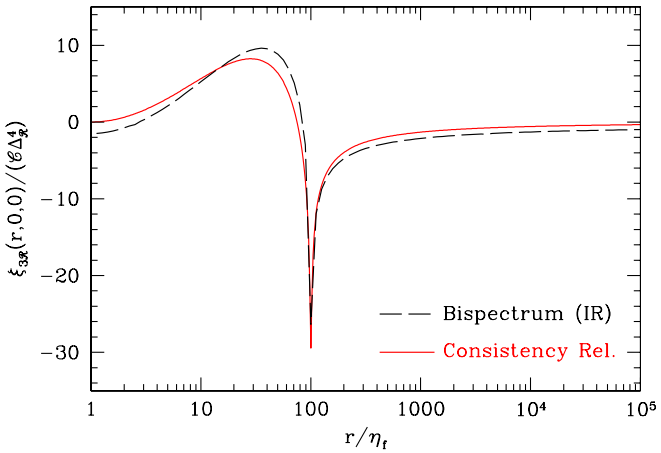

FIG. 16 (color online). The contribution to the real space three-point correlation function from the infrared terms (the second two terms) in Eq. (A25) (dashed black curve) and the consistency relation of Eq. (A35) (red solid curve). We take $x_d = 100$ with an infrared cutoff at $k_{\rm min} = 0.001/\eta_f$.

This is consistent with the findings of Sec. IV B, where it was shown that perturbative validity places a weak constraint of $c/d < 10^4$ such that a finite step cannot have infinitesimal width.

APPENDIX B: SLOW ROLL CORRECTIONS TO THE BISPECTRUM

In this Appendix we show that one of the largest and simplest corrections to the bispectrum can be associated with the difference in phase between the slow roll spacetime and de Sitter space. This phase difference leads to a real component of the growing mode on superhorizon scales. We show that these slow roll corrections are largely responsible for the 10% error in the approximations in Sec. IV.

In deriving the expression for the bispectrum, Eq. (48), we used only the de Sitter form for the mode function $y(x)$, which is related to the curvature perturbation by

$$\mathcal{R}_k = \sqrt{\frac{2\pi^2}{k^3}}\frac{xy(x)}{f}. \tag{B1}$$

Here $x = k\eta$ and $y(x)$ is the solution of the Mukhanov-Sasaki equation,

$$\frac{d^2y}{dx^2} + \left(1 - \frac{2 + g(\ln x)}{x^2}\right)y = 0, \tag{B2}$$

where

$$g(\ln x) = \frac{f'' - 3f'}{f}, \tag{B3}$$

and primes denote derivatives with respect to $\ln x$. In the de Sitter limit, $g = 0$, and

$$y(x) = \left(1 + \frac{i}{x}\right)e^{ix}. \tag{B4}$$

In this approximation, for modes that are outside the horizon, $x \ll 1$, the growing mode of y which yields the constant part of the curvature $\mathcal{R}$ is purely imaginary, while the real component decays as x^2 in this limit. Writing the bispectrum in Eq. (45) as

$$\begin{aligned} B_{\mathcal{R}}(k_1,k_2,k_3) \approx & -4{\rm Im}[\mathcal{R}_{k_1}(\eta_*)\mathcal{R}_{k_2}(\eta_*)\mathcal{R}_{k_3}(\eta_*)] \\ & \times {\rm Re}\Big[\int_{\eta_*}^{\infty}\frac{d\eta}{\eta^2}a^2\epsilon_H(\epsilon_H - \eta_H)' \\ & \times (\mathcal{R}^*_{k_1}\mathcal{R}^*_{k_2}\mathcal{R}^*_{k_3})'\Big] \\ & - 4\,{\rm Re}[\mathcal{R}_{k_1}(\eta_*)\mathcal{R}_{k_2}(\eta_*)\mathcal{R}_{k_3}(\eta_*)] \\ & \times {\rm Im}\Big[\int_{\eta_*}^{\infty}\frac{d\eta}{\eta^2}a^2\epsilon_H(\epsilon_H - \eta_H)' \\ & \times (\mathcal{R}^*_{k_1}\mathcal{R}^*_{k_2}\mathcal{R}^*_{k_3})'\Big], \end{aligned} \tag{B5}$$

we expect that the bispectrum is dominated by the first term, whereas the second term should be of order $\mathcal{O}(\epsilon_H)$.

Since $\epsilon_H \sim 0.01$, one may expect that neglecting the slow roll corrections amounts to a small percent level correction to the leading order bispectrum. However, as we will see the coefficient in front of these terms is such that the correction is on the order of 10% (see also [27]).

In the limit where the inflaton is slowly rolling down its potential, the function $g(\ln x)$ is smooth, slowly varying and $\mathcal{O}(n_s - 1)$. The scalar fluctuations, governed by Eq. (B2), begin as plane waves $y \propto e^{ix}$ in Minkowski space at $x \gg \infty$ before they begin to feel the expansion when their wavelength becomes comparable to the horizon, $x \sim 1$, where they begin to grow as $y \propto 1/x$ for $x \ll 1$. As long as g is slowly varying, the only time it is important is when the mode crosses the horizon. Thus for a given wave number k, to a good approximation, we can Taylor expand about the time of horizon crossing, and to a first approximation, write

$$\frac{d^2y}{dx^2} + \left(1 - \frac{2 + g_0}{x^2}\right)y = 0, \tag{B6}$$

where $g_0 = g(x = 1)$ is a function of k, but is time independent. In this limit, Eq. (B6) can be solved exactly. Demanding that y is asymptotically a positive frequency plane wave as $x \to \infty$ implies that

$$y(x) = -e^{-i(\pi\nu/2)+i(3\pi/2)}\sqrt{\frac{\pi x}{2}}H_\nu^{(1)}(x), \tag{B7}$$

where $H_\nu^{(1)}(x)$ is the Hankel function of the first kind and

$$\nu = \frac{1}{2}\sqrt{9 + 4g_0} \approx \frac{3}{2} + \frac{g_0}{3}. \tag{B8}$$

Now, as described in Sec. IV, the bispectrum due to a step feature in the potential is dominated by modes that are deep inside the horizon when the inflaton crosses the feature. At early times, the modes are identical to the de Sitter modes, at leading order in x, while at late times, expanding the Hankel function one finds

$$\begin{aligned} xy(x) &\to ie^{-i(\pi\nu/2)+i(3\pi/2)}\Gamma(\nu)\sqrt{\frac{2}{\pi}}\left(\frac{2}{x}\right)^{\nu-(3/2)} \\ &\approx i + i\frac{[2 - \gamma - \ln(2) - \ln(x)]}{3}g_0 + \frac{\pi g_0}{6} \\ &\quad + \mathcal{O}(x^2, g_0^2). \end{aligned} \tag{B9}$$

The growing mode on superhorizon scales is no longer purely imaginary. There is also a correction to the amplitude of the imaginary part of the growing mode; however, note that we have already taken this correction into account by using the square root of Eq. (22) in Eq. (48) which contains slow roll corrections in $\Delta^2_{\mathcal{R},0}$. In this approximation, in the superhorizon limit, $xy(x)$ is not only not constant but diverges as $\ln(x)$. However, it is easy to see that the curvature perturbation, defined in Eq. (B1), is actually constant in this limit. The assumption that $g = \text{const}$ implies that the function f has time dependence

$$f \approx f_0\left[1 - \frac{g_0}{3}\ln(x)\right] + \mathcal{O}(g_0^2), \tag{B10}$$

to leading order in g_0, which is precisely the right behavior to cancel out the time dependence of Eq. (B9).

In the limit of large momenta, corresponding to modes well inside the horizon, the leading order (in k and slow roll) correction to the bispectrum is given by

$$\begin{aligned} B_{\mathcal{R}}^{(1)}(k_1, k_2, k_3) \approx &-\frac{(2\pi)^4}{k_1^2k_2^2k_3^2}\frac{\Delta_{\mathcal{R}}(k_1)\Delta_{\mathcal{R}}(k_2)\Delta_{\mathcal{R}}(k_3)}{4} \\ &\times \frac{\pi}{2}g_0 I_3(K), \end{aligned} \tag{B11}$$

where

$$I_3(K) = \int_{\eta_*}^{\infty}\frac{d\eta}{\eta}G_B'(\ln\eta)K\eta\cos(K\eta). \tag{B12}$$

In the same approximation as Sec. IV, we can evaluate this integral to obtain

$$I_3(K) = \frac{\mathcal{C}}{2f_0}\mathcal{D}\left(\frac{\pi d}{2\sqrt{2\epsilon_0}}K\eta_f\right)X_3(K\eta_f), \tag{B13}$$

where

$$\begin{aligned} X_3(K) = &-\frac{(x^4 - 9x^2 + 54)\sin(x)}{x^2} \\ &+ \frac{(-2x^4 + 27x^2 - 54)\cos(x)}{x^3} + \frac{54}{x^3}. \end{aligned} \tag{B14}$$

Relative to the dominant zeroth order term [the X_0 term of Eq. (55)] the main contribution from this slow roll correction is $\pi/2$ out of phase, but has the same envelope. Notice also that, in the limit $x \to 0$, this window function vanishes only as $X_3(x) \sim \mathcal{O}(x)$, compared to $\mathcal{O}(x^2)$ for the window functions of Eq. (55). This implies that, at sufficiently small x, this correction will eventually dominate the leading order result. This is not particularly surprising given that we have only considered the dominant correction in the high momentum limit. Near the horizon scale at feature crossing, $k\eta_f = 1$, many other terms become equally, if not more important.

The upper panel of Fig. 17 shows a comparison between the analytic approximation to this first order term, Eqs. (B11) and (B14) and the second term in Eq. (B5) for a step with height $c = 10^{-5}$ and width $d = 0.001$. The prefactor for this term varies slowly over the range of wave numbers considered, and we take the value $\pi g_0/2 = 0.1$ which is near the middle of its range for this plot. The lower panel in Fig. 17 shows the fractional error on the full bispectrum when this term is added to the analytic approximation of Sec. IV. While the approximation is improved significantly at large k, the improvement gets steadily worse as the horizon scale is approached. This is to be

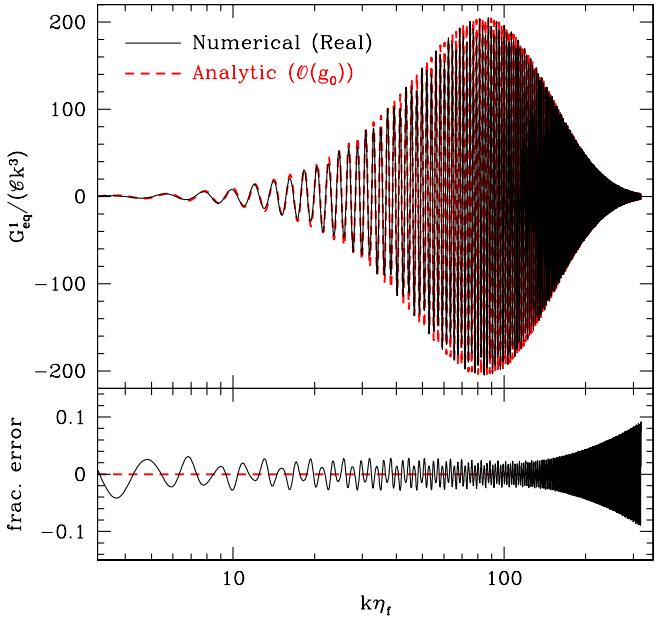

FIG. 17 (color online). First order corrections to the equilateral bispectrum computed using the analytic approximation Eqs. (B11) and (B14) compared with the numerical evaluation of the second term in Eq. (B5) for a step with height $c = 10^{-5}$ and width $d = 0.001$. The lower panel here shows the fractional error of the full bispectrum, once this first order correction is taken into account. We take $\pi g_0/2 = 0.1$ for this plot.

expected, given that we have not attempted to calculate all of the terms that are important for modes that are near the horizon as the feature is crossed.

We also note that these corrections are important for the power spectrum of Sec. III [2]. In particular, note that the squeezed limit consistency relation (see Sec. IV C) implies that there should be a correction to the power spectrum of the same order of magnitude. We leave the calculation of further slow roll corrections to future work.

Before we end this section, we clarify one point that may confuse the reader. In deriving the correction Eq. (B9), at first glance it appears that the prefactor is simply an irrelevant global phase that will simply cancel once all terms are taken into account. Indeed, the bispectrum is constructed out of the two-point functions which always involve the pair

$$\langle \hat{\mathcal{R}}_{\mathbf{k}}(\eta)\hat{\mathcal{R}}_{\mathbf{k}'}(\tilde{\eta})\rangle = \mathcal{R}_k(\eta)\mathcal{R}^*_k(\tilde{\eta})(2\pi)^3\delta^3(\mathbf{k}+\mathbf{k}'). \tag{B15}$$

However, if one were to choose to cancel the phase in each propagator, one would of course obtain the same answer. While the growing mode would be purely imaginary outside the horizon, at very early times the mode would look as if it initially started with a phase shift relative to the de Sitter space modes, leading to the same correction we have calculated here.

APPENDIX C: SEPARABILITY

Separability of the bispectrum into products of functions that depend only on the individual k_i's is desirable in that the angular bispectrum can then also be constructed from separate ℓ_i calculations using the full radiation transfer function instead of the flat-sky Sachs-Wolfe expressions used in the main text.

The formulation of the eigenmode decompositions of Fergusson, Liguori, and Shellard [39,40] which allow for the projection of nonseparable bispectra onto a (band-limited) complete basis of separable functions has largely ameliorated the need for the bispectra themselves to be separable. However, for a polynomial basis of degree n, one can only accurately fit a function with n zero crossings, and thus, it seems that projection of the highly oscillatory functions considered here might prove to be very inefficient with this method. Polynomials, however, are not the only such basis that has been proposed; the oscillatory basis of Meerburg [41] would perhaps be more suited for this type of bispectra. Nonetheless, in this Appendix, we point out that the analytic form of the bispectrum derived above is, to a very good approximation, separable.

The bispectrum from Eqs. (48), (54), and (55) appears to be inseparable due to the fact that the damping factor appears to depend on the perimeter of the triangle in momentum space

$$\mathcal{D}(x) = \frac{x}{\sinh x}, \qquad x = \sum_{i=1}^{3} x_i, \tag{C1}$$

where $x_i = k_i\eta_f(\pi d/2\sqrt{2\epsilon_0})$. This cannot be exactly written in the form

$$\mathcal{D}(x) = \prod_{i=1}^{3}\mathcal{D}_i(x_i). \tag{C2}$$

We can, however, approximate the damping factor in this form. First note that at $x \gg 1$

$$\lim_{x\gg 1}\mathcal{D}(x) = 2xe^{-x}(1+e^{-2x}), \tag{C3}$$

which is separable. In the opposite limit, the damping factor vanishes as x^2 whereas the expansion goes as $4x$. To fix this problem we take

$$\mathcal{D}(x) \approx 2xe^{-x}(1+e^{-2x}) + e^{-4x}, \tag{C4}$$

which is of the form of a sum of separable components since $e^{-x} = \prod_i e^{-x_i}$. The remaining inseparable $1/K^n$ type factors that appear in the window functions can be written in separable form by introducing Schwinger parameters as described in [42]. However, we note that the terms that require this treatment are subdominant, and to a reasonable approximation away from $K = 0$, the bispectrum is dominated by terms that are separable.

[1] J. Choe, J.-O. Gong, and E. D. Stewart, J. Cosmol. Astropart. Phys., 07 (2004) 012.
[2] C. Dvorkin and W. Hu, Phys. Rev. D **81**, 023518 (2010).
[3] C. Dvorkin and W. Hu, Phys. Rev. D **82**, 043513 (2010).
[4] C. Dvorkin and W. Hu, Phys. Rev. D **84**, 063515 (2011).
[5] R. Flauger and E. Pajer, J. Cosmol. Astropart. Phys. 01 (2011) 017.
[6] L. Leblond and E. Pajer, J. Cosmol. Astropart. Phys. 01 (2011) 035.
[7] A. A. Starobinsky, JETP Lett. **55**, 489 (1992) [http://www.jetpletters.ac.ru/ps/1276/article_19291.shtml].
[8] H. Peiris *et al.* (WMAP Collaboration), Astrophys. J. Suppl. Ser. **148**, 213 (2003).
[9] L. Covi, J. Hamann, A. Melchiorri, A. Slosar, and I. Sorbera, Phys. Rev. D **74**, 083509 (2006).
[10] J. Hamann, L. Covi, A. Melchiorri, and A. Slosar, Phys. Rev. D **76**, 023503 (2007).
[11] M. J. Mortonson, C. Dvorkin, H. V. Peiris, and W. Hu, Phys. Rev. D **79**, 103519 (2009).
[12] X. Chen, R. Easther, and E. A. Lim, J. Cosmol. Astropart. Phys. 06 (2007) 023.
[13] X. Chen, R. Easther, and E. A. Lim, J. Cosmol. Astropart. Phys. 04 (2008) 010.
[14] S. Hotchkiss and S. Sarkar, J. Cosmol. Astropart. Phys. 05 (2010) 024.
[15] F. Arroja, A. E. Romano, and M. Sasaki, Phys. Rev. D **84**, 123503 (2011).
[16] J. Martin and L. Sriramkumar, arXiv:1109.5838.
[17] P. Adshead, W. Hu, C. Dvorkin, and H. V. Peiris, Phys. Rev. D **84**, 043519 (2011).
[18] E. D. Stewart, Phys. Rev. D **65**, 103508 (2002).
[19] R. Bean, X. Chen, G. Hailu, S.-H. Tye, and J. Xu, J. Cosmol. Astropart. Phys. 03 (2008) 026.
[20] J. M. Maldacena, J. High Energy Phys. 05 (2003) 013.
[21] S. Weinberg, Phys. Rev. D **72**, 043514 (2005).
[22] J. A. Adams, B. Cresswell, and R. Easther, Phys. Rev. D **64**, 123514 (2001).
[23] X. Chen, arXiv:1104.1323.
[24] X. Chen, Phys. Lett. B **706**, 111 (2011).
[25] P. Creminelli and M. Zaldarriaga, J. Cosmol. Astropart. Phys. 10 (2004) 006.
[26] P. Creminelli, G. D'Amico, M. Musso, and J. Norena, J. Cosmol. Astropart. Phys. 11 (2011) 038.
[27] C. Burrage, R. H. Ribeiro, and D. Seery, J. Cosmol. Astropart. Phys. 07 (2011) 032.
[28] H. C. Chiang *et al.*, Astrophys. J. **711**, 1123 (2010).
[29] M. L. Brown *et al.* (QUaD Collaboration), Astrophys. J. **705**, 978 (2009).
[30] See http://www.supernova.lbl.gov/Union.
[31] A. G. Riess *et al.*, Astrophys. J. **699**, 539 (2009).
[32] S. Burles, K. M. Nollett, and M. S. Turner, Astrophys. J. **552**, L1 (2001).
[33] J. Martin and C. Ringeval, Phys. Rev. D **69**, 083515 (2004).
[34] R. Flauger, L. McAllister, E. Pajer, A. Westphal, and G. Xu, J. Cosmol. Astropart. Phys. 06 (2010) 009.
[35] P. Meerburg, R. Wijers, and J. P. van der Schaar, arXiv:1109.5264.
[36] W. Hu, Phys. Rev. D **62**, 043007 (2000).
[37] P. Creminelli, L. Senatore, and M. Zaldarriaga, J. Cosmol. Astropart. Phys. 03 (2007) 019.
[38] D. Babich and M. Zaldarriaga, Phys. Rev. D **70**, 083005 (2004).
[39] J. Fergusson, M. Liguori, and E. Shellard, Phys. Rev. D **82**, 023502 (2010).
[40] J. R. Fergusson, M. Liguori, and E. P. S. Shellard, arXiv:1006.1642.
[41] P. Meerburg, Phys. Rev. D **82**, 063517 (2010).
[42] K. M. Smith and M. Zaldarriaga, Mon. Not. R. Astron. Soc. **417**, 2 (2011).